energies

MDPI

Article

Impact of Distributed Generators Penetration Level on the Power Loss and Voltage Profile of Radial Distribution Networks

Sunday Adeleke Salimon [1,*], Gafari Abiola Adepoju [1], Isaiah Gbadegesin Adebayo [1,*], Harun Or Rashid Howlader [2,*], Samson Oladayo Ayanlade [3] and Oludamilare Bode Adewuyi [4]

[1] Department of Electronic and Electrical Engineering, Ladoke Akintola University of Technology, Ogbomoso 212102, Nigeria
[2] Faculty of Engineering, University of the Ryukyus, 1 Senbaru, Nakagami, Nishihara-cho 903-0213, Okinawa, Japan
[3] Department of Electrical and Electronic Engineering, Lead City University, Ibadan 200255, Nigeria
[4] Faculty of Engineering, Information and Systems, University of Tsukuba, 1 Chrome-1-1 Tennodai, Tsukuba 305-8577, Ibaraki, Japan
* Correspondence: sasalimon@lautech.edu.ng (S.A.S.); igadebayo@lautech.edu.ng (I.G.A.); h.h.howlader@ieee.org (H.O.R.H.)

Abstract: The Distributed Generator types have different combinations of real and reactive power characteristics, which can affect the total power loss and the voltage support/control of the radial distribution networks (RDNs) in different ways. This paper investigates the impact of DG's penetration level (PL) on the power loss and voltage profile of RDNs based on different DG types. The DG types are modeled depending on the real and reactive power they inject. The voltage profiles obtained under various circumstances were fairly compared using the voltage profile index (VPI), which assigns a single value to describe how well the voltages match the ideal voltage. Two novel effective power voltage stability indices were developed to select the most sensitive candidate buses for DG penetration. To assess the influence of the DG PL on the power loss and voltage profile, the sizes of the DG types were gradually raised on these candidate buses by 1% of the total load demand of the RDN. The method was applied to the IEEE 33-bus and 69-bus RDNs. A PL of 45–76% is achieved on the IEEE 33-bus and 48–55% penetration on the IEEE 69-bus without an increase in power loss. The VPI was improved with increasing PL of DG compared to the base case scenario.

Keywords: distributed generation (DG); radial distribution network (RDN); penetration level (PL); voltage profile index (VPI); power loss

Citation: Salimon, S.A.; Adepoju, G.A.; Adebayo, I.G.; Howlader, H.O.R.; Ayanlade, S.O.; Adewuyi, O.B. Impact of Distributed Generators Penetration Level on the Power Loss and Voltage Profile of Radial Distribution Networks. *Energies* **2023**, *16*, 1943. https://doi.org/10.3390/en16041943

Academic Editor: Hugo Morais

Received: 8 January 2023
Revised: 10 February 2023
Accepted: 12 February 2023
Published: 15 February 2023

1. Introduction

The distribution system is the last stage that connects the end-users (consumers) of electricity and the electrical power system [1]. The topological structure of most distribution systems is usually designed to be radial in topography due to low cost, more accessible protection, easier voltage control, and easier power flow control, while few are weakly meshed [2]. Though the radial distribution network (RDN) allows a unidirectional flow of power from the substation to the consumers and has the advantages mentioned earlier, it is plagued with severe technical issues of huge power losses, and large voltage drops, thereby making the distribution system the weakest link and the least reliable section of the power system. It has been estimated that about 13% of the total power generated is wasted as losses in the power system, and the distribution system accounts for about 70% of these losses [3]. The massive distribution loss is due to the topological and structural characteristics of the distribution networks, including the radiality or weakly meshed nature of the system, the composition of unbalanced load, high resistance to reactance (R/X) compared to the transmission system, and the presence of many components [4]. The penetration of an appropriate size of distributed generation (DG) at strategic location(s)

is one method to improve the efficiency, reliability, and performance of the distribution network, as inappropriate allocation may worsen the situation [5].

Distributed Generation (DG) can be defined as small-scale, dispersed, or embedded generation connected directly to the distribution grid [6]. DG units are based on conventional (non-renewable) and renewable sources. DG technologies such as internal combustion engines, gas turbines, and microturbines are associated with non-renewable (conventional) energy sources. In contrast, renewable DG technologies are solar PV, wind, fuel cells, small hydro, biomass, solar thermal, and geothermal systems [7]. The advantages of integrating DGs into the distribution system include decreased line losses; better voltage profile; stability; and power quality; increased network efficiency; reliability improvement; security enhancement; diminished transmission and distribution (T & D) congestion; delayed investments for facility upgrades; decrease in loss expenses associated with lowered operational and maintenance costs; and eradication of fuel costs for DGs [8]. At high penetration levels, though, the existence of DG in the distribution network may also impose various issues and restrictions, including overvoltage situations and higher system losses [9,10]. Finding the best places for DG units to be integrated into the system without requiring significant structural changes is the key difficulty, as this will ensure that all bus voltage levels remain within acceptable ranges [11].

Penetration is a percentage-based or dynamic measurement of the power magnitude produced or provided by incorporated DG compared to all other generating resources on a power network during a certain period of load [12]. A tiny proportion of DG penetration during peak demand could represent a significant degree of penetration under low load, proving that penetration is not a static metric. The penetration level of DG can be determined subject to the following constraints: voltage deviation, network loss, and total harmonic distortion limits. The issues mentioned above become incredibly important as DG penetration levels rise. In order to guarantee the proper and dependable power network operation with considerable quantities of DG, voltage stability analysis will ultimately be required [13,14]. Voltage instability can easily happen when the power system is under stress (for example, due to an increase in load). The weakest bus is where this kind of voltage instability most frequently happens [15]. Consequently, finding the location and degree of DG penetration presents difficult planning and management problems for the system; and this has prompted researchers to use optimization techniques to obtain the actual penetration level and optimal location of DG for various technical and economic benefits [16]. Nevertheless, it is also imperative to study how a steady increment in the penetration levels of DG compared to the source generation affects the voltage profile, power loss, and other derivable benefits of the network. Therefore, this study will show vividly how the variation of DG penetration level affects these benefits and give the exact size of DG that will yield maximum benefit, which can serve as a benchmark for verification of the optimal values of DG obtained from optimization techniques.

2. Literature Review, Research Gap and Contribution of the Study

Researchers at different stages of research have proposed numerous classical and optimization approaches to obtain the actual penetration level and location of DG for minimal power, improvement of voltage profile, and maximization of other benefits. Some of the population-based optimization techniques include particle swarm optimization [17], modified acquila optimizer (MAO) [18], improved wild horse optimization (IWHO) [19], political optimization algorithm (POA) [20], Honey Badger Algorithm (HBA) [21], whale optimization algorithm (WOA) [22], ant-lion optimization (ALO) [23], new oppositional hybrid sine cosine muted differential evolution algorithm (NOHSCMDEA) [24], and so on.

The authors of [25] proposed a hybrid of analytical and particle swarm optimization approach for optimal integration of distributed generators (DG) and distribution network reconfiguration to maximize the power loss reduction and DG penetration level (PL) increment while keeping the voltage profile improvement within the permissible limit. Ref. [26] has worked on the impact of DG on the losses and voltage magnitudes of the grids

at various penetration levels (PLs). The work revealed that the extent to which DGs affect losses and voltage depends on the DG technology. Moreover, it was shown that the PL of DG reduces the power loss until a threshold point, after which the losses begin to increase. By considering the voltage limitations on all buses and assessing their effects on the network losses and voltage profile, the DG penetration levels were raised. In [27], an analytical method was proposed to determine the maximum distributed generator penetration in the existing power system without increasing the total power loss. The maximum DG penetration levels were calculated using the base case voltages in the analytical expression.

In [28], the penetration level of the DG was evaluated for the maximum loadability and minimum power loss of the RDN using a novel load pattern-based voltage stability index. It was discovered that it is essential to consider the system loadability of the RDN alongside studying the power loss reduction, voltage profile improvement, and the voltage stability index to determine the DG penetration level. The authors in [29] examined the impact level of photovoltaic power plant and wind power plant penetration into an IEEE 9-bus system considering frequency, voltage, and fault level of DG. The results show that the system performs well while penetration is under 30% of the total load of the grid. Ref. [30] analyzed the effect of photovoltaic distributed generator (PVDG) numbers on RDN power losses and voltage profiles at various penetration levels. In terms of voltage profile, it was found that the voltage profile has improved by connecting a higher number of PVDG units. Furthermore, this increase in voltages keeps growing while increasing the penetration level. On the other side, the power loss reduction has also been raised by injecting more PVDG units. The authors in [31] analyzed how the penetration level of shunt capacitor (SC) affects the techno-economic benefits derivable from integrating SC into RDNs. The techno-economic benefits under consideration were the power loss, voltage profile, and net savings. The results showed that appropriate penetration of SC leads to a reduction of power losses, voltage profile improvement as well as cost reduction.

In [32], which examined the voltage profile of secondary systems under conservation voltage minimization and DG penetration, in-depth modeling of three power system networks in New York City were deployed as the case studies. The study found dispersed networks with DG implemented had better voltage management, enabling utilities to employ deeper voltage reductions in emergencies. Additionally, it was shown that when DG penetration is high, the network power factor decreases; as a result, the line drop compensation must be changed to account for the increased power demand. Reference [33] examined the impacts of DG installation on the operation of the distribution system, including a voltage magnitude analysis, losses, and the system cost. The influence of dispersing the DG over the bus where the load is most significant and different sizes of DG penetration levels were investigated in the technique. The voltage profile, real power losses, and system cost were also examined. Ref. [34] suggested modifying the Jaya algorithm (JA) to determine each PV system's optimal capacity, which would improve the voltage magnitudes and minimize the loss at high penetration levels.

Ref. [35] proposed a bio-geography-based algorithm (BBA) for allocating multiple DG for power loss minimization and voltage profile improvement. In [36], the authors presented Voltage Stability Margin Index (VSMI) for the selection of weak buses, and curve fitting approximation was utilized to determine the size of the DG to minimize the power loss and improve the voltage stability of the distribution network. The impact of DG on shunt-compensated radial medium voltage networks has been investigated by [37]. The authors of [38] have examined the impact of varying distributed energy resources (DER) penetration on the distribution system's reliability and voltage profile improvement. In [39], the analysis of increasing penetration level of solar photovoltaic DG units on power loss, voltage profile, and overloading of the distribution system was carried out. Ref. [40] proposed a dual stage for the allocation of fuel cells. In the first stage, the location was determined using a neural network, whereas the second stage utilized Artificial Bee Colony (ABC) to size the DG. The literature review is summarized in Table 1.

Table 1. Summary of Literature Review.

S/N	Ref.	Objectives	Optimization/Solution Method	DG Type/Limitation
1.	[17]	Power loss	PSO	Type 1 DG only
2.	[18]	Power loss and voltage deviation (VD)	MAO	Types 1 and 2 DGs only
3.	[19]	Power loss	IWHO/Evaluation of reliability assessment	Type 2 DG only
4.	[20]	Power loss	VSI and POA	Types 1–3 DG only
5.	[21]	Power loss	HBA	VD was not considered
6.	[22]	Power loss	WOA	Types 1–3 DGs
7.	[23]	Power loss, VD, VSI	ALO	Types 1–2 DGs
8.	[24]	Power loss, VD, VSI	NOHSCMDEA	Types 1 -2 DGs
9.	[25]	Power loss	NVSI & PSO	Type 1 DG
10.	[26]	Power loss, VD	Analytical PL	Types 1–3 DGs
11.	[27]	Power loss	Analytical	Type 1 DG
12.	[28]	Power loss, loadability	Analytical/Determined maximum PL	Type 1 DG
13.	[29]	Frequency, Voltage, Fault level	Analytical/PL	Types 1 and 3 DGs
14.	[30]	Power loss, voltage profile	Analytical/PL	Type 1 DG
15.	[31]	Power loss, VD, cost	Increasing PL	Type 4 DG
16.	[32]	Voltage profile	Analytical	Type 1 DG
17.	[33]	Power loss, voltage profile, cost	Analytical/PL	Type 1 DG
18.	[34]	Voltage and power loss	JA	Type 1 DG
19.	[35]	Voltage profile and power loss	BBA	Type 1 DG
20.	[36]	Voltage stability and losses	VSMI & curve fitting approximation	Types 1 and 2 DGs
21.	[37]	Voltage profile	Load flow sensitivities	Type 1 DG
22.	[38]	Reliability and VD	Monte Carlo simulation	Type 1 DG
23.	[39]	Power loss, voltage profile, overloading	Increasing PL	Type 1 DG
24.	[40]	Power loss, VSI, VD	ABC	Type 1 DG

As mentioned above, most studies modeled DG as a device solely capable of producing real power. Only a few authors, including [26], investigated how three DG technologies affect a sub-transmission network. DGs are categorized into four classes depending on the terminal and electrical characteristics of the actual and reactive power they inject into the power system [41]. They are mainly integrated at the distribution level [42]. Varied combinations of the reactive power characteristics included in these DG types can affect the power network's overall loss and voltage support/control in diverse ways. It is important to remember that the DG type chosen will significantly impact how well the power network works. These DG types have different combinations of real and reactive power characteristics, which can affect the power system's total power loss and voltage support/control in different ways. Thus, the type of DG technology adopted will have a significant bearing on the performance of the power network and benefits derivable from the installation of DG. Hence, looking at how different DG types affect overall loss and voltage magnitudes is crucial to reap the system-wide advantages.

This research aimed to investigate how four different DG types at different penetration levels affected the radial distribution network's (RDN) power loss and voltage profile. Novel Effective Real Power Voltage Stability Index (EPVSI) and Effective Reactive Power Voltage Stability Index (EQVSI) are developed to select the first five most sensitive buses to compensation since the nodes of distribution networks are numerous. Thus, to find out how the penetration level of DGs affects the loss and voltage magnitudes of the radial distribution network, the DG technology types are connected one at a time to the chosen buses, with the penetration level changing in steps of 1% increments up until the full load (maximum point). In order to assist in the extension of the maximum penetration limit of DG to create a sustainable power system, this study is helpful for power system engineers in distribution network planning and operation. Furthermore, the study's optimal values

may be utilized to verify the optimal solutions to DG or capacitor allocation issues found using any optimization method.

The following are the study's significant contributions:

- Development of novel EPVSI and EQVSI for selection of most sensitive candidate buses for real and reactive compensation. These analytical indices can also reduce the search space for DG or capacitor placement before using the population-based optimization method to determine the optimal allocation.
- Modeling the four DG types with a novel model for the reactive-based DG synchronous machine (Condenser) from the principle of the synchronous model, which is helpful for the load flow of distribution and sub-transmission networks.
- The study determines how the penetration level of various DG types affects critical technical advantages, including power loss and voltage profile.
- The study's outcome can be used as a benchmark for confirming the optimal values of DG and capacitor allocation problems.
- Implementation on the IEEE 33-bus and 69-bus radial distribution network.

3. Types and Modelling of the Distributed Generators

As indicated in [41], *DG*s can also be categorized into four primary categories based on their electrical terminal features in terms of real and reactive power providing capacities. In Table 2, the four *DG* kinds taken into consideration for this study are presented with examples.

Table 2. *DG* Technology Types and Classes [41].

DG Type	Electrical Characteristics	DG technology	Examples
Type 1	Injects P only	Asynchronous generator	Solar PV, fuel cell
Type 2	Injects both P and Q	Synchronous generator	Internal combustion engines, gas turbines, steam turbines, microturbines,
Type 3	Injects P and absorbs Q	Induction generator	Squirrel cage induction generator (wind generator)
Type 4	Injects only Q	Synchronous generator	Synchronous condenser

Generators integrated into the power system can be modeled as either PQ nodes or PV nodes. Small DGs (Induction or Synchronous) are approximately modeled as PQ nodes and are usually taken as negative constant power loads [43] as shown in Figure 1.

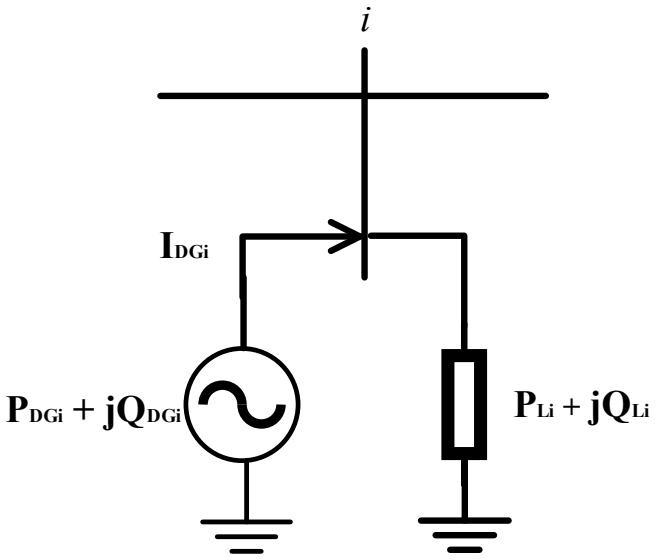

Figure 1. A *DG* and a *PQ* load connected to a bus *i*.

The load is approximated as a continuous power load, and its current is provided as:

$$I_{Li} = \left(\frac{P_{Li} + jQ_{Li}}{V_i}\right)^* \quad (1)$$

While the current injected by the *DG* is given as:

$$I_{DGi} = \left(\frac{P_{DGi} + jQ_{DGi}}{V_i}\right)^* \quad (2)$$

3.1. Type 1 DG—Power Converter Interface Model

The Type 1 *DG*s need a power electronic converter interface to connect to the grid, as seen in Figure 2. The real and the reactive power may be controlled by maintaining the modulation depth of the power conditioning unit (PCU) (Ψ) and the advance angle of the PCU (M), respectively [44]. It is operated in voltage control mode with limited reactive power as either PQ or PV node [44]. If the real power of the *DG* at node i is given as, then the apparent and reactive are given as:

$$|S| = \frac{P_{DGi}}{pf} \text{ and } Q_{DGi} = \sqrt[2]{S^2 - P_{DGi}^2} \quad (3)$$

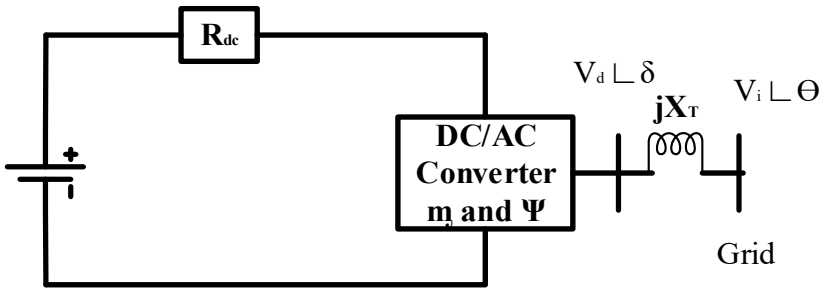

Figure 2. Circuit Diagram of power converter interface.

The *DG* shifts from PV to PQ mode and maintains the reactive power restrictions if the computed reactive power exceeds the top limits. The value is taken as one for the Type 1 DG; hence, only real is injected while injected reactive power is zero.

3.2. Type 2 DG—Power Converter Interface Model

Real and reactive power are both added to the power system by the synchronous generator. A PQ node is modeled as the synchronous generator when it is used in power factor control mode [44]. The power factor can be controlled by controlling the excitation current. The equivalent synchronous generator model is shown in Figure 3. Given that P_{DGi} are the *DG* real power and the power factor under which the *DG* will operate is pf_{Gi}, so the reactive power, Q_{DG}, is given as:

$$Q_{DGi} = P_{DGi} \tan(cos^{-1}(pf_{DGi})) \quad (4)$$

$$Q_{DGi} = V_i\left(\frac{E_{DGi} - V_G}{X_{DGi}}\right) \quad (5)$$

3.3. Type 3 DG—Induction Generator Model

The induction generator can be modeled based on ratings and generator parameters as a PQ node [43]. The final induction generator equivalent circuit is illustrated in Figure 4.

$$\text{Let } X_s = X_a + X_b \text{ and } X_P = \frac{X_{cX_m}}{X_c - X_m} \quad (6)$$

$$P_{DGi} + jQ_{DGi} = \frac{V^2}{Z} \tag{7}$$

$$V_i = \sqrt{\frac{-P_{DGi}\left(s^2X_s^2 + R_2^2\right)}{R_2 s}} \tag{8}$$

$$\text{Therefore, } Q_{DGi} = -\frac{V_i^2}{X_p} + \frac{-V_i^2 + \sqrt{V_i^4 - 4P_{DGi}^2X_s^2}}{2X_s} \tag{9}$$

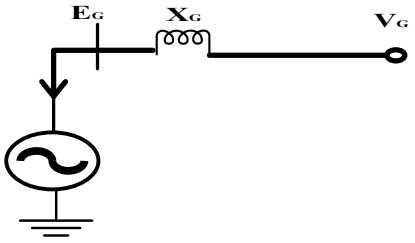

Figure 3. Equivalent circuit of synchronous generator.

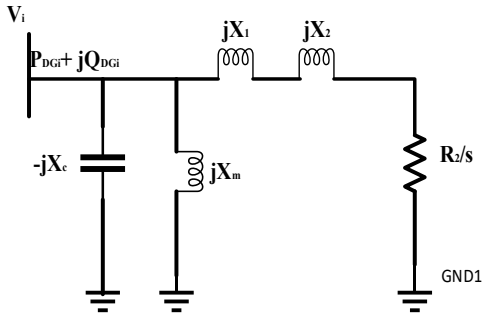

Figure 4. Equivalent circuit of induction generator.

3.4. Type 4 DG—Synchronous Condenser Model

The synchronous condenser injects or absorbs reactive power depending on the excitation of the field current with no real power output as a PQ node. They can be modeled as synchronous generators but with no steady-state active power output. Except that there is no prime mover, the representation of a synchronous condenser is similar to that of a synchronous generator.

The equivalent steady-state representation of a simple synchronous machine model connected to bus 'i' is shown in Figure 5. The steady-state model of synchronous machines assumes a constant field current. This model neglect saliency effects and stator resistance and offers considerable structural and computational simplicity.

$$\overline{E_q} = \overline{V_i} + jX_S\overline{I_{DG}} \tag{10}$$

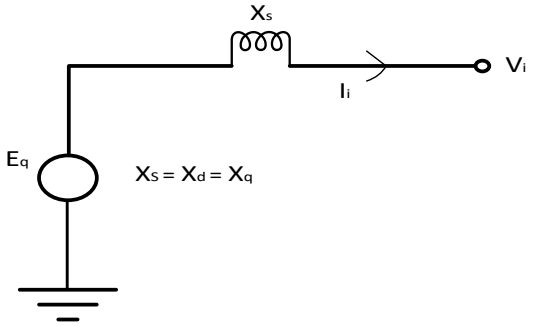

Figure 5. Steady State Model of Synchronous Machine.

The e.m.f. E_q generated in the armature or stator of a synchronous machine is proportional to excitation of the field current, i_{fd} of the rotor, hence

$$|E_q| = X_{ad} i_{fd} \tag{11}$$

Equating the components along and perpendicular to the phasor V_i, results in

$$\left(X_{ad} i_{fd}\right) \sin \partial = X_S I_i \cos \sigma \tag{12}$$

$$\left(X_{ad} i_{fd}\right) \cos \partial = V_i + X_S I_i \sin \sigma \tag{13}$$

Multiplying the equations with V_i and equating P = 0 (no real power output for synchronous condenser) gives

$$Q_{DGi} = \frac{X_{ad}}{X_S} V_i i_{fd} - \frac{V_i^2}{X_S} \tag{14}$$

4. Derivation of Effective Real and Reactive Power Voltage Stability Index (EPVSI and EQVSI) for Selection of Sensitive Candidate Buses

The New Voltage Stability Index (NVSI) proposed by [45] is modified to formulate the EPVSI and EQVSI by utilizing the effective power emanating from each bus in the index rather than power injection at each bus. This will represent the power flow through each distribution line more accurately and give an index very sensitive to both voltage collapse and power loss reduction for DG integration. The proposed index was utilized to determine the nodes for DG penetration and ranked them according to how sensitive they are to voltage breakdown.

Considering a sample distribution system illustrated in Figure 6 with a total of '*N*' nodes and a distribution line (branch) '*m-n*' is mapped out for the formulation of the EPVSI where '*m*' represents the sending end node and '*n*' represents the receiving end node as depicted in Figure 6.

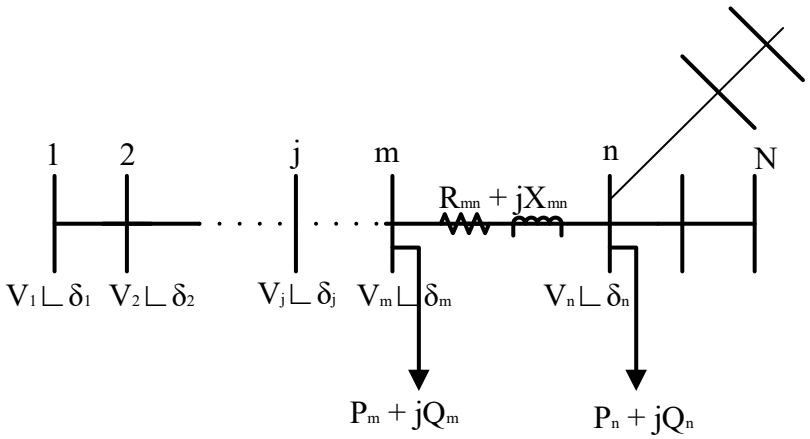

Figure 6. A sample distribution system showing details of distribution line '$m-n$'.

The branch current, I_{mn} can be calculated by Equation (15)

$$I_{mn} = \left(\frac{P_{n\,eff} + jQ_{n\,eff}}{V_n \angle \delta_n}\right)^* \tag{15}$$

where $P_{n\,eff}$ and $Q_{n\,eff}$ = effective sum of the real and reactive power demands, respectively of all buses emanating from bus '*n*'.

The voltage at the receiving end can be expressed as

$$V_n \angle \delta_n = V_m \angle \delta_m - (R_{mn} + jX_{mn}) I_{mn}$$
$$V_n \angle \delta_n = V_m \angle \delta_m - (R_{mn} + jX_{mn}) \left(\frac{P_{n\ eff} + jQ_{n\ eff}}{V_n \angle \delta_n} \right)^*$$
$$V_n^2 = V_m V_n \angle (\delta_m - \delta_n) - (R_{mn} + jX_{mn}) \left(P_{n\ eff} - jQ_{n\ eff} \right)$$

Let $(\delta_m - \delta_n) = 0$

$$V_n^2 - V_m V_n + P_{n\ eff} R_{mn} + Q_{n\ eff} X_{mn} + j\left(Q_{n\ eff} R_{mn} - P_{n\ eff} X_{mn} \right) = 0$$

Separate and equate the real and imaginary parts to zero

$$V_n^2 + P_{n\ eff} R_{mn} + Q_{n\ eff} X_{mn} = V_m V_n \tag{16}$$

$$Q_{n\ eff} R_{mn} - P_{n\ eff} X_{mn} = 0 \tag{17}$$

$$R_{mn} = \frac{P_{n\ eff} X_{mn}}{Q_{n\ eff}} \tag{18}$$

Put Equation (18) into (16)

$$V_n^2 - V_m V_n + \left(\frac{P_{n\ eff}^2 + Q_{n\ eff}^2}{Q_{n\ eff}} \right) X_{mn} = 0 \tag{19}$$

For stable bus voltages, the discriminant, $D = b^2 - 4ac$ of the quadratic equation in Equation (19) must be greater than or equal to zero, that is,

$$V_m^2 - 4 \left(\frac{P_{n\ eff}^2 + Q_{n\ eff}^2}{Q_{n\ eff}} \right) X_{mn} \ \geq 0 \tag{20}$$

$$1 \geq \frac{4X_{mn}}{V_m^2} \left(\frac{P_{n\ eff}^2 + Q_{n\ eff}^2}{Q_{n\ eff}} \right) \tag{21}$$

$$EPVSI_{(m-n)} = \frac{4X_{m-n}}{V_m^2} \left(\frac{P_{n,eff}^2 + Q_{n,eff}^2}{Q_{n,eff}} \right) \leq 1 \tag{22}$$

Similarly, by substituting X_{mn} from Equation (17) into Equation (16), *EQVSI* can be derived as

$$EQVSI_{(m-n)} = \frac{4R_{m-n}}{V_m^2} \left(\frac{P_{n,eff}^2 + Q_{n,eff}^2}{P_{n,eff}} \right) \leq 1 \tag{23}$$

The values of *EPVSI* and *EQVSI* should be smaller than unity under typical operating circumstances. The system will be more stable if the value is nearer to zero. A high *EPVSI* (or *EQVSI*) score indicates that the system is unstable. The bus that has a high *EPVSI* (or *EQVSI*) value is more sensitive and is chosen as a candidate bus for DG penetration when its voltage is less than 0.95 [46].

The effective real and reactive power demand of all buses can be obtained with the aid of the simple line diagram in Figure 7.

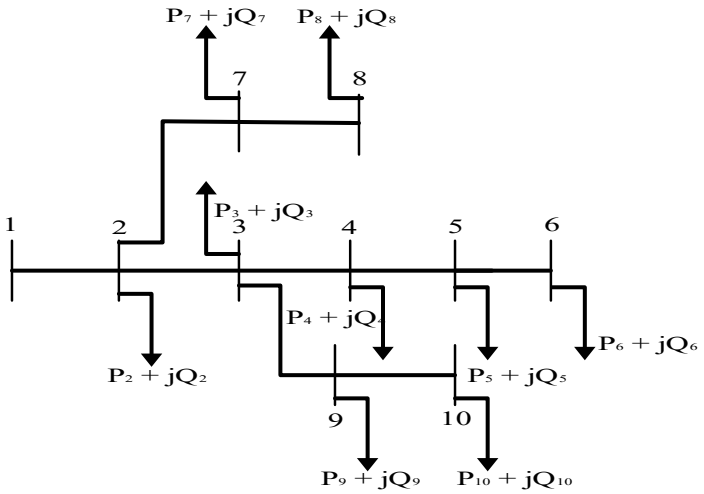

Figure 7. A simple radial distribution network.

From Figure 7,

$$\left.\begin{array}{c} P_{10,eff} = P_{10} \\ P_{9,eff} = P_9 + P_{10} \\ P_{8,eff} = P_8 \\ P_{7,eff} = P_7 + P_8 \\ P_{6,eff} = P_6 \\ P_{5,eff} = P_5 + P_6 \\ P_{4,eff} = P_4 + P_5 + P_6 \\ P_{3,eff} = P_3 + P_4 + P_5 + P_9 + P_{10} \\ P_{2,eff} = P_2 + P_3 + P_4 + P_5 + P_9 + P_{10} \end{array}\right\} \quad (24)$$

$$\begin{bmatrix} P_{2,\text{eff}} \\ P_{3,\text{eff}} \\ P_{4,\text{eff}} \\ P_{5,\text{eff}} \\ P_{6,\text{eff}} \\ P_{7,eff} \\ P_{8,\text{eff}} \\ P_{9,\text{eff}} \\ P_{10,eff} \end{bmatrix} = \begin{bmatrix} 1 & 1 & 1 & 1 & 1 & 1 & 1 & 1 & 1 \\ 0 & 1 & 1 & 1 & 1 & 0 & 0 & 1 & 1 \\ 0 & 0 & 1 & 1 & 1 & 0 & 0 & 0 & 0 \\ 0 & 0 & 0 & 1 & 1 & 0 & 0 & 0 & 0 \\ 0 & 0 & 0 & 0 & 1 & 0 & 0 & 0 & 0 \\ 0 & 0 & 0 & 0 & 0 & 1 & 1 & 0 & 0 \\ 0 & 0 & 0 & 0 & 0 & 0 & 1 & 0 & 0 \\ 0 & 0 & 0 & 0 & 0 & 0 & 0 & 1 & 1 \\ 0 & 0 & 0 & 0 & 0 & 0 & 0 & 0 & 1 \end{bmatrix} \begin{bmatrix} P_2 \\ P_3 \\ P_4 \\ P_5 \\ P_6 \\ P_7 \\ P_8 \\ P_9 \\ P_{10} \end{bmatrix} \quad (25)$$

The following is an expression of Equation (22)'s general form:

$$\left[P_{effM}\right] = [BIBC][P_{RM}] \quad (26)$$

Similarly,

$$\left[Q_{effM}\right] = [BIBC][Q_{RM}] \quad (27)$$

where P_{effM} = effective real power matrix of the total distribution system

P_{RM} = real power demand matrix of the total distribution network
Q_{effM} = effective reactive power matrix of the total distribution network
Q_{RM} = reactive power demand matrix of the total distribution network
BIBC = bus injection to branch current matrix

The BIBC matrix can be built or computed for any distribution system using the steps stated and diagrammatically depicted in Figure 8 for MATLAB programming. The example illustrated for the determination of the BIBC matrix in Figure 9 is carried out using Figure 7.

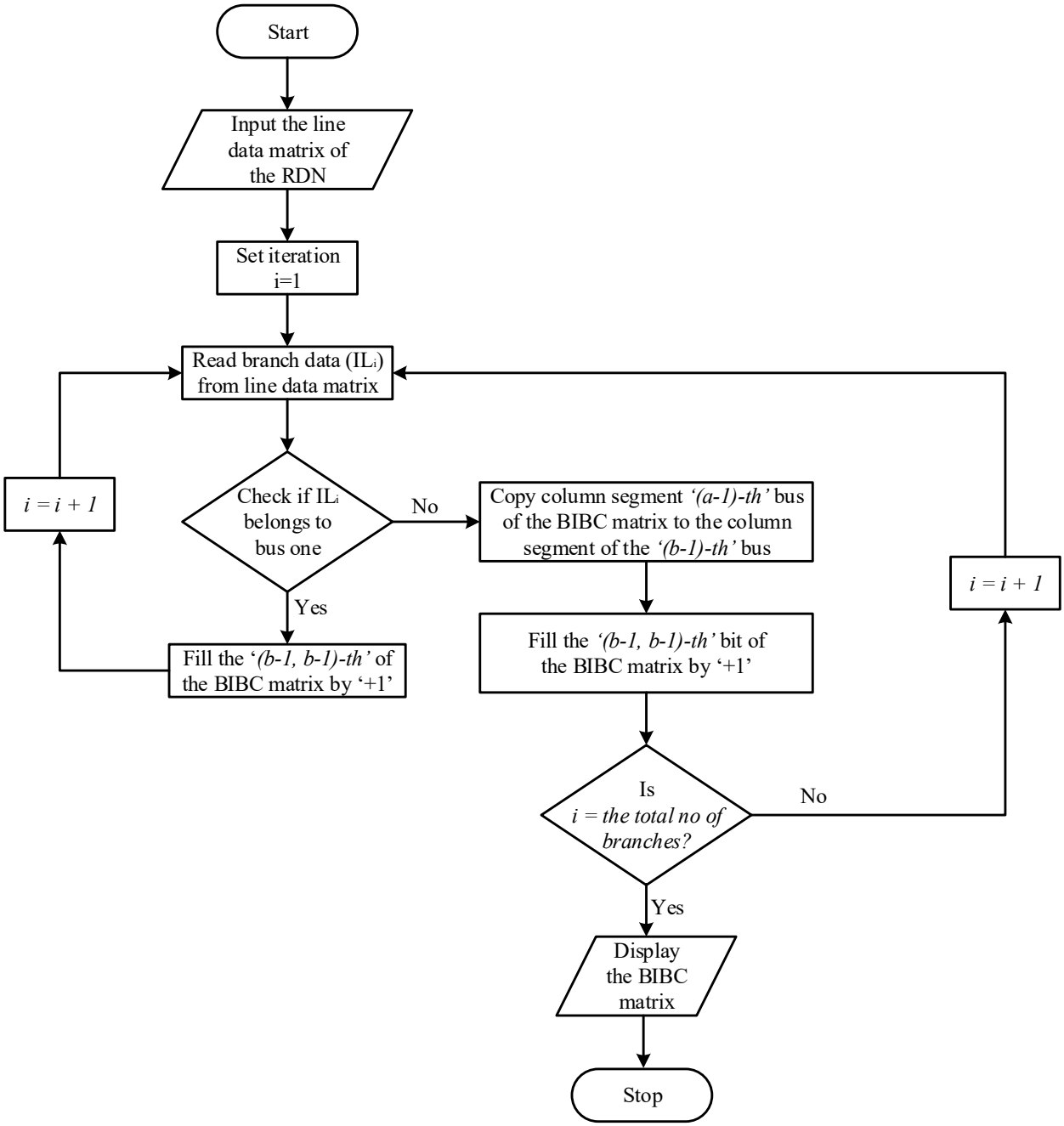

Figure 8. Procedural steps for the formation of the BIBC matrix.

Step 1: Given a RDN with 'x' number of branches and 'y' number of buses, create a null BIBC matrix with dimension $(x \times (y-1))$

Step 2: Set i = 1 and read the branch data from the line data matrix. If a branch (IL_i) is positioned between bus 'a' and 'b' and belongs (connected) to bus '1', then fill the (*b-1*, *b-1*)-*th* bit of the BIBC matrix by '+1'. Increment 'i' by one or go to step #3.

Step 3: If the branch (IL_i) is not connected to the first bus, then copy the '*(a-1)-th*' bus of the BIBC matrix to the column segment of '*(b-1)-th*' bus and fill the (*b-1*, *b-1*)-*th* bit of the BIBC matrix by '+1'. Increment 'i' by one and return to step 2. Figure 9 explains this.

Step 4: Repeat step 2 and step 3 until $i = x$ which signifies the completion of the BIBC matrix. At this stage, all the branches of the RDN would have been included in the BIBC matrix.

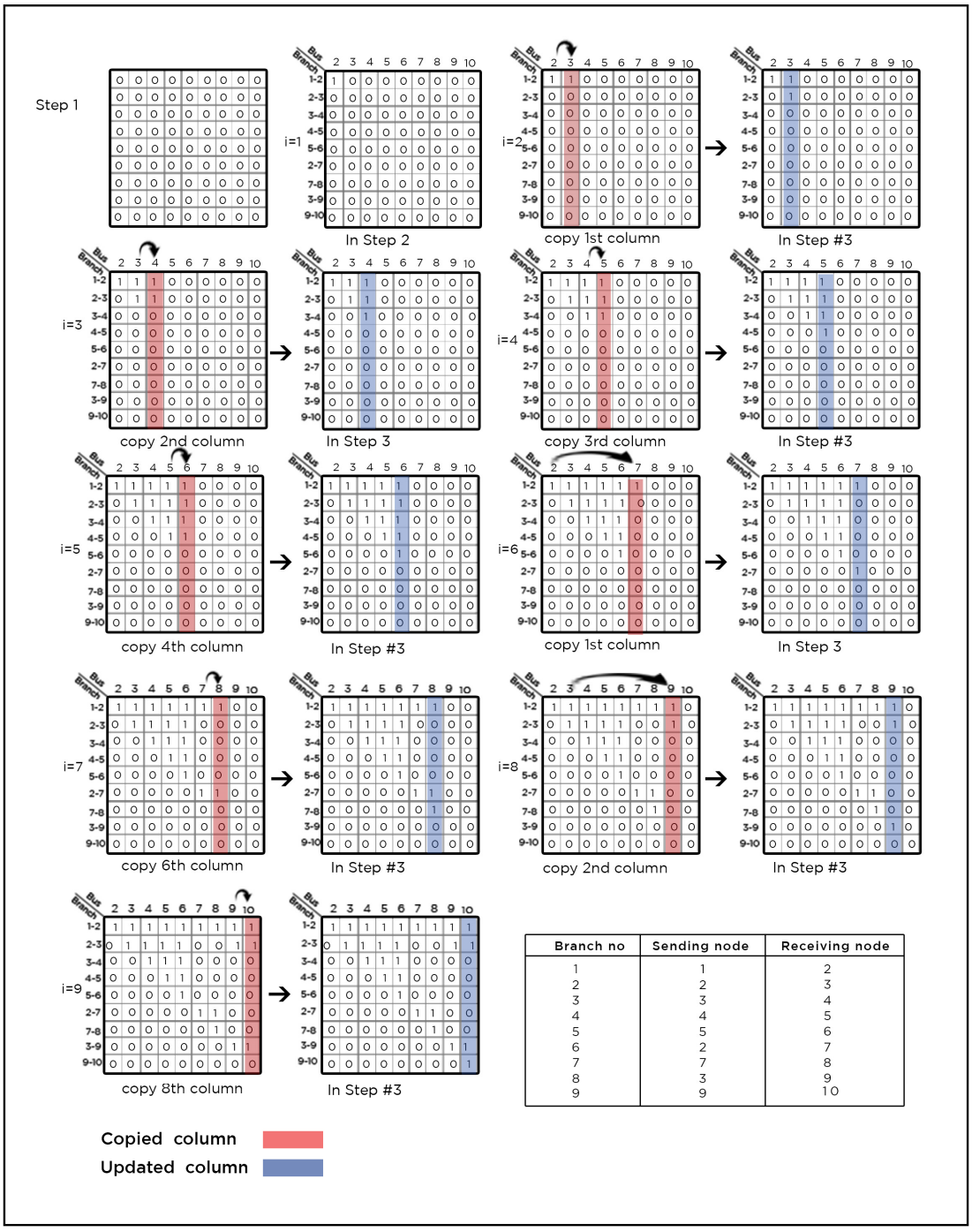

Branch no	Sending node	Receiving node
1	1	2
2	2	3
3	3	4
4	4	5
5	5	6
6	2	7
7	7	8
8	3	9
9	9	10

Figure 9. The formation of BIBC matrix using the simple distribution system.

5. Determining the Impacts of DG Types on the Power System

The effects of the various DGs on the distribution networks were quantified using the real and reactive losses resulting from their interconnection to the system and the impact of that connection on the voltage profile.

5.1. Determination of Losses in the Radial Distribution Network

The real and reactive power losses can be calculated after obtaining the current flowing through the transmission line from the load flow analysis.

$$Ploss = I_i^2 R \tag{28}$$

$$Qloss = I_i^2 X \tag{29}$$

5.2. Determination of Voltage Profile Index

An index suggested by [26] to provide a single value to describe how closely the voltage fits the ideal was used to compare the voltage profiles obtained from various circumstances. The mathematical definition of the Voltage Profile Index (*VPI*) is as follows:

$$VPI = \left(c \times \left| \frac{1}{V_m - 1} \right| \right) \tag{30}$$

V_m and c can be determined as follows:

$$V_m = \frac{1}{N_b} \sum_{i=1}^{N_b} V_i \tag{31}$$

$$c = 1 - V_\tau \tag{32}$$

$$V_\tau = \sqrt{\frac{1}{N} \sum_{i=1}^{N_b} (V_i - V_m)^2} \tag{33}$$

where N_b = number of buses, N_b = bus voltage magnitude i, V_m = network mean voltage, V_τ = bus voltage deviation. For instance, let the VPI of scenario x be VPI_X and that of scenario y be VPI_Y. If $VPI_X > VPI_Y$, then it means the overall voltage profile of 'x' is better than 'y'.

5.3. Penetration Level

The percentage of the network's real load demand that is satisfied by the real power produced by the DG types is referred to as the penetration level (PL) in this study [47]. It is the proportion of electricity the DG generates to the network's overall power requirement. The network's ability to function must not be compromised by the DG's percentage penetration.

$$\% \text{ Penetration Level} = \frac{P_{DG}}{P_{load}} \times 100\% \tag{34}$$

P_{DG} can be any of Type 1, Type 2, or Type 3 *DG*s. For Type 4 *DG*, the penetration level for the proposed type 4 *DG* model is expressed as:

$$\% \text{ Penetration Level} = \frac{Q_{DG}}{Q_{load}} \times 100\% \tag{35}$$

5.4. Determination of Candidate Buses for DG Penetration

The radial distribution network to be used to determine the impact of the different DG types consists of numerous PQ buses and a slack bus. The candidate buses on which the DG types was placed in order to analyze their impact was determined using sensitivity analysis as given in the step below:

Step 1: Perform the base case's load flow.

Step 2: Using the formulae provided in Equations (20) and (21), calculate the EPVSIs and EQVSIs at the distribution networks' buses.

Step 3: Compute the normalized voltage magnitude V_N [46] of the buses by the Equation (32).

$$V_N = \frac{V_i}{0.95} \tag{36}$$

Step 3: Rank the EPVSI (or EQVSI) of the buses whose normalized voltage magnitude V_N is less than 1.01 in descending order. These are the most sensitive buses to DG or capacitor placement.

Step 4: Select the first five ranked candidate buses for DG type penetration.

5.5. Steps for Determination of DG Types Impact

The procedure for the determination of impacts of the DG types on the power system is illustrated in the flowcharts of Figure 10 for the radial distribution networks. Many scenarios were developed to better understand the potential effects of DGs on the electricity networks. A situation in which there are no interconnected DGs is represented by the base case. By interconnecting several DG types in succession and then raising their penetration level, additional scenarios were obtained.

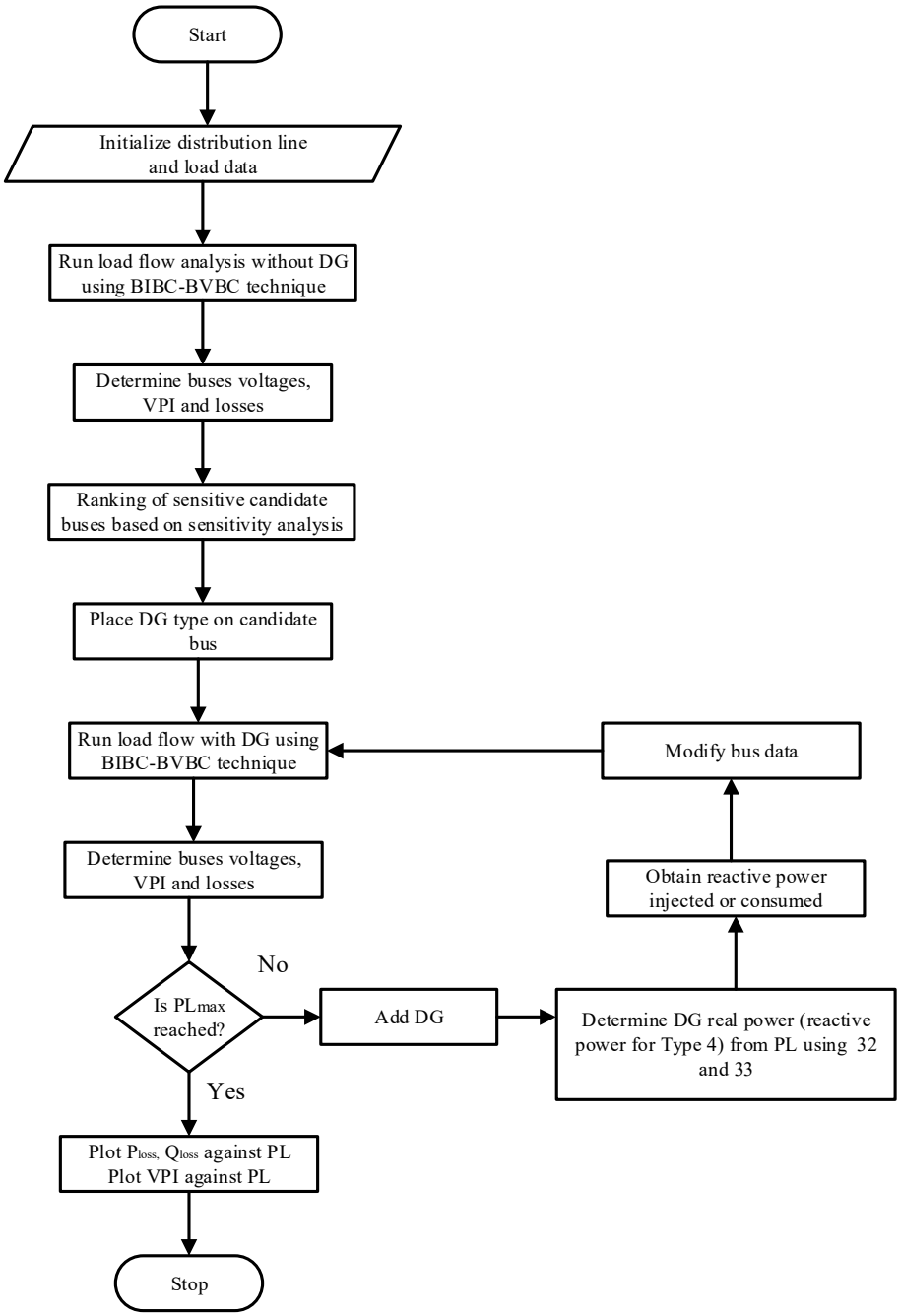

Figure 10. Flow chart to obtain the impact of DG types on Radial Distribution Network.

6. Results and Discussion

The DG penetration level effect on losses and voltage profiles in the distribution networks was investigated using simulations. The implementation program codes were developed using the MATLAB program to tackle the power flow issues with and without DG integration. The developed approach was assessed on IEEE 33 and 69-bus networks derived from [48,49]. Two scenarios were considered to demonstrate the potential effects of the DG on the effectiveness of the distribution system. The first scenario represents the Base Case (BC), or situation in which no DG was added to the system. The second scenario is a situation in which the penetration level is enhanced after the DG is interconnected to the distribution system using a variety of buses chosen from the top five listings of the EPVSI and EQVSI results acquired from the base case.

6.1. Base Case and Selection of Candidate Buses Using EPVSI and EQVSI

The BC scenario enables comparison with the DG placement scenario. The simulation was run for BC, and Table 3 provides the overall real and reactive power demand and losses, as well as *VPI*. Table 3 indicates that the real and reactive losses were 211 kW and 143 kVar, respectively, and the voltage profile index for the IEEE 33-bus network was 1.25. For the IEEE 69-bus network, the real and reactive losses, and the VIP, were 1.563, 225 kW, and 102 kVar, respectively.

Table 3. Base Case Scenario Results.

Parameter (Units)	IEEE 33	IEEE 69
Total load demand (kW)	3715	3802.0
Total load demand (kVar)	2300	2694.0
Total real power loss (kW)	211.00	225.0
Total reactive power loss (kVar)	143.00	102.1
VPI	1.25	1.563

After the base case simulation, the *EPVSI* and *EQVSI* values obtained for the IEEE 33-bus and 69-bus systems are illustrated in Figures 11 and 12. The results of EPVSI and EQVSI for IEEE 33-bus and IEEE 69-bus RDNs are shown in Tables 4 and 5, respectively. From Figure 11a, the first five buses with the highest ranking were buses 6, 13, 8, 7, and 28, with corresponding EPVSI values ($\times 10^{-3}$) of 80.5304, 75.2974, 45.3196, 40.2157, and 37.7198, respectively for the 33-bus network while that of the 69-bus network were buses 57, 58, 61, 60 and 59 with corresponding EPVSI values ($\times 10^{-3}$) of 49.78832, 24.82707, 23.35775, 10.50488, and 9.540518, respectively as depicted in Figure 11b. Similarly, the first five buses for EQVSI are buses 6, 28, 8, 29, and 30 with values ($\times 10^{-3}$) of 67.1853, 51.3142, 48.883, 38.7497, and 23.0603, respectively, for the 33-bus network. The selected buses for the IEEE 69-bus system using the EQVSI formula were buses 57, 58, 61, 60, and 59 with the corresponding values ($\times 10^{-3}$) of 105.9369, 52.8371, 37.7341, 24.7034, and 20.64041. These are the first five weakest buses most sensitive to loss-reduction based on the EPVSI formula used in the method for the Type 1–3 DGs, while the buses selected by the EQVSI were used for the Type 4 DG. As a result, they were chosen for connection and DG penetration. The findings for real losses, reactive losses, and VPI when all of the four DG types were connected to the selected buses in turn at rising penetration levels are examined in the following sub-sections.

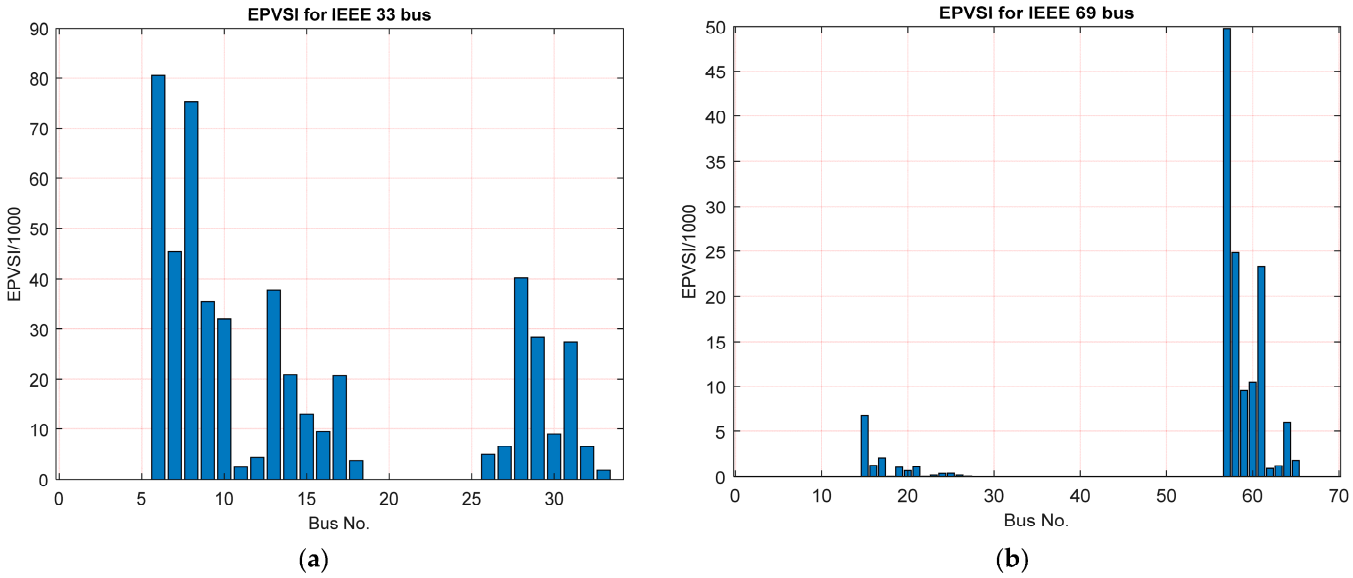

(**a**) (**b**)

Figure 11. EPVSI values for IEEE (**a**) 33-bus (**b**) 69-bus RDNs.

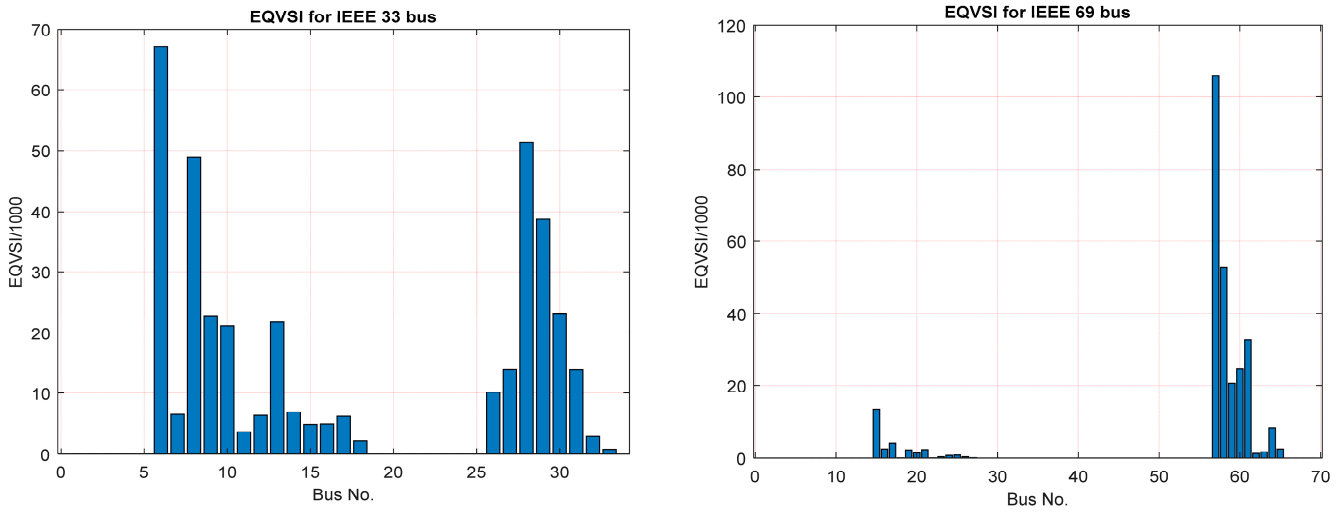

(**a**) (**b**)

Figure 12. EQVSI values for IEEE (**a**) 33-bus (**b**) 69-bus RDNs.

Table 4. Results of EPVSI and EQVSI for IEEE 33-bus RDN.

Line No	From Bus (f)	To Bus (t)	V(f)	V(t)	$V_N = \frac{V(t)}{0.95}$	EPVSI $\times 10^{-3}$	Ranking 1 (EPVSI)	EQVSI $\times 10^{-3}$	Ranking 2 (EQVSI)
1	1	2	1.0000	0.9970	1.0495	-	-	-	-
2	2	3	0.9970	0.9829	1.0346	-	-	-	-
3	3	4	0.9829	0.9754	1.0267	-	-	-	-
4	4	5	0.9754	0.9679	1.0189	-	-	-	-
5	5	6	0.9679	0.9495	0.9994	80.5304	1	67.1853	1
6	6	7	0.9495	0.9459	0.9957	45.3196	3	6.5043	13
7	7	8	0.9459	0.9323	0.9814	75.2974	2	48.8883	3
8	8	9	0.9323	0.9260	0.9747	35.4973	6	22.6913	6
9	9	10	0.9260	0.9201	0.9685	31.9993	7	21.2063	8
10	10	11	0.9201	0.9192	0.9676	2.4898	20	3.6635	18
11	11	12	0.9192	0.9177	0.9660	4.4567	18	6.3426	14
12	12	13	0.9177	0.9115	0.9595	37.7198	5	21.8401	7

Table 4. *Cont.*

Line No	From Bus (f)	To Bus (t)	V(f)	V(t)	$V_N=\frac{V(t)}{0.95}$	EPVSI $\times 10^{-3}$	Ranking 1 (EPVSI)	EQVSI $\times 10^{-3}$	Ranking 2 (EQVSI)
13	13	14	0.9115	0.9092	0.9571	20.8338	10	6.8993	12
14	14	15	0.9092	0.9078	0.9556	13.0143	12	4.8742	17
15	15	16	0.9078	0.9064	0.9541	9.4722	13	4.9413	16
16	16	17	0.9064	0.9044	0.9520	20.6589	11	6.1893	15
17	17	18	0.9044	0.9038	0.9513	3.8437	19	2.1786	20
18	2	19	0.9970	0.9965	1.0489	-	-	-	-
19	19	20	0.9965	0.9929	1.0452	-	-	-	-
20	20	21	0.9929	0.9922	1.0444	-	-	-	-
21	21	22	0.9922	0.9916	1.0438	-	-	-	-
22	3	23	0.9829	0.9793	1.0308	-	-	-	-
23	23	24	0.9793	0.9726	1.0238	-	-	-	-
24	24	25	0.9726	0.9693	1.0203	-	-	-	-
25	6	26	0.9495	0.9475	0.9974	5.0137	17	10.1641	11
26	26	27	0.9475	0.9450	0.9947	6.5905	15	13.9226	9
27	27	28	0.9450	0.9335	0.9827	40.2158	4	51.3142	2
28	28	29	0.9335	0.9253	0.9740	28.3872	8	38.7497	4
29	29	30	0.9253	0.9218	0.9703	8.9907	14	23.0602	5
30	30	31	0.9218	0.9176	0.9659	27.5016	9	13.9136	10
31	31	32	0.9176	0.9167	0.9649	6.5100	16	2.8961	19
32	32	33	0.9167	0.9164	0.9646	1.8771	21	0.8049	21

Table 5. Results of EPVSI and EQVSI for IEEE 69-bus RDN.

Line No	From Bus (f)	To Bus (t)	V(f)	V(t)	$V_N=\frac{V(t)}{0.95}$	EPVSI	Ranking 1 (EPVSI)	EQVSI	Ranking 2 (EQVSI)
1	1	2	1.0000	1.0000	1.0526	-	-	-	-
2	2	3	1.0000	0.9999	1.0526	-	-	-	-
3	3	4	0.9999	0.9998	1.0525	-	-	-	-
4	4	5	0.9998	0.9990	1.0516	-	-	-	-
5	5	6	0.9990	0.9901	1.0422	-	-	-	-
6	6	7	0.9901	0.9808	1.0324	-	-	-	-
7	7	8	0.9808	0.9786	1.0301	-	-	-	-
8	8	9	0.9786	0.9774	1.0289	-	-	-	-
9	9	10	0.9774	0.9724	1.0236	-	-	-	-
10	10	11	0.9724	0.9713	1.0225	-	-	-	-
11	11	12	0.9713	0.9682	1.0191	-	-	-	-
12	12	13	0.9682	0.9653	1.0161	-	-	-	-
13	13	14	0.9653	0.9624	1.0130	-	-	-	-
14	14	15	0.9624	0.9595	1.0009	6.7580	6	13.4809	6
15	15	16	0.9595	0.9590	1.0094	1.2572	10	2.5064	10
16	16	17	0.9590	0.9581	1.0085	2.0774	8	4.1409	8
17	17	18	0.9581	0.9581	1.0085	0.0212	21	0.0422	21
18	18	19	0.9581	0.9576	1.0080	1.0520	13	2.2618	13
19	19	20	0.9576	0.9573	1.0077	0.6704	15	1.4545	15
20	20	21	0.9573	0.9568	1.0072	1.0910	12	2.3484	12
21	21	22	0.9568	0.9568	1.0072	0.0155	22	0.0336	22
22	22	23	0.9568	0.9568	1.0071	0.1625	18	0.3510	18
23	23	24	0.9568	0.9566	1.0069	0.3537	17	0.7641	17
24	24	25	0.9566	0.9564	1.0068	0.3823	16	0.8262	16
25	25	26	0.9564	0.9564	1.0067	0.1577	19	0.3409	19
26	26	27	0.9564	0.9563	1.0067	0.0442	20	0.0956	20
27	3	28	0.9999	0.9999	1.0526	-	-	-	-
28	28	29	0.9999	0.9999	1.0525	-	-	-	-
29	29	30	0.9999	0.9997	1.0524	-	-	-	-
30	30	31	0.9997	0.9997	1.0523	-	-	-	-

Table 5. *Cont.*

Line No	From Bus (f)	To Bus (t)	V(f)	V(t)	$V_N = \frac{V(t)}{0.95}$	EPVSI	Ranking 1 (EPVSI)	EQVSI	Ranking 2 (EQVSI)
31	31	32	0.9997	0.9996	1.0522	-	-	-	-
32	32	33	0.9996	0.9993	1.0519	-	-	-	-
33	33	34	0.9993	0.9990	1.0516	-	-	-	-
34	34	35	0.9990	0.9989	1.0515	-	-	-	-
35	3	36	0.9999	0.9999	1.0525	-	-	-	-
36	36	37	0.9999	0.9998	1.0524	-	-	-	-
37	37	38	0.9998	0.9996	1.0522	-	-	-	-
38	38	39	0.9996	0.9996	1.0522	-	-	-	-
39	39	40	0.9996	0.9996	1.0522	-	-	-	-
40	40	41	0.9996	0.9989	1.0514	-	-	-	-
41	41	42	0.9989	0.9986	1.0511	-	-	-	-
42	42	43	0.9986	0.9985	1.0511	-	-	-	-
43	43	44	0.9985	0.9985	1.0511	-	-	-	-
44	44	45	0.9985	0.9984	1.0510	-	-	-	-
45	45	46	0.9984	0.9984	1.0510	-	-	-	-
46	4	47	0.9998	0.9998	1.0524	-	-	-	-
47	47	48	0.9998	0.9985	1.0511	-	-	-	-
48	48	49	0.9985	0.9947	1.0471	-	-	-	-
49	49	50	0.9947	0.9942	1.0465	-	-	-	-
50	8	51	0.9786	0.9785	1.0300	-	-	-	-
51	51	52	0.9785	0.9785	1.0300	-	-	-	-
52	9	53	0.9774	0.9747	1.0260	-	-	-	-
53	53	54	0.9747	0.9714	1.0225	-	-	-	-
54	54	55	0.9714	0.9669	1.0178	-	-	-	-
55	55	56	0.9669	0.9626	1.0132	-	-	-	-
56	56	57	0.9626	0.9401	0.9896	49.7883	1	105.9369	1
57	57	58	0.9401	0.9290	0.9779	24.8271	2	52.8371	2
58	58	59	0.9290	0.9248	0.9734	9.5405	5	20.6041	5
59	59	60	0.9248	0.9197	0.9681	10.5049	4	24.7034	4
60	60	61	0.9197	0.9123	0.9604	23.3577	3	32.7341	3
61	61	62	0.9123	0.9121	0.9601	0.9127	14	1.2794	14
62	62	63	0.9121	0.9117	0.9596	1.2222	11	1.7128	11
63	63	64	0.9117	0.9098	0.9576	6.0059	7	8.4105	7
64	64	65	0.9098	0.9092	0.9570	1.8175	9	2.5403	9
65	11	66	0.9713	0.9713	1.0224	-	-	-	-
66	66	67	0.9713	0.9713	1.0224	-	-	-	-
67	12	68	0.9682	0.9679	1.0188	-	-	-	-
68	68	69	0.9679	0.9679	1.0188	-	-	-	-

6.2. Impact of Type 1 DG on the Radial Distribution Network

The Type 1 DG was successively installed in many carefully selected buses. Figures 13–15 show the outcomes for active power and reactive power losses as well as VPI when Type 1 DG was installed at the vulnerable buses of both IEEE 33 and 69-bus while the penetration level was gradually raised.

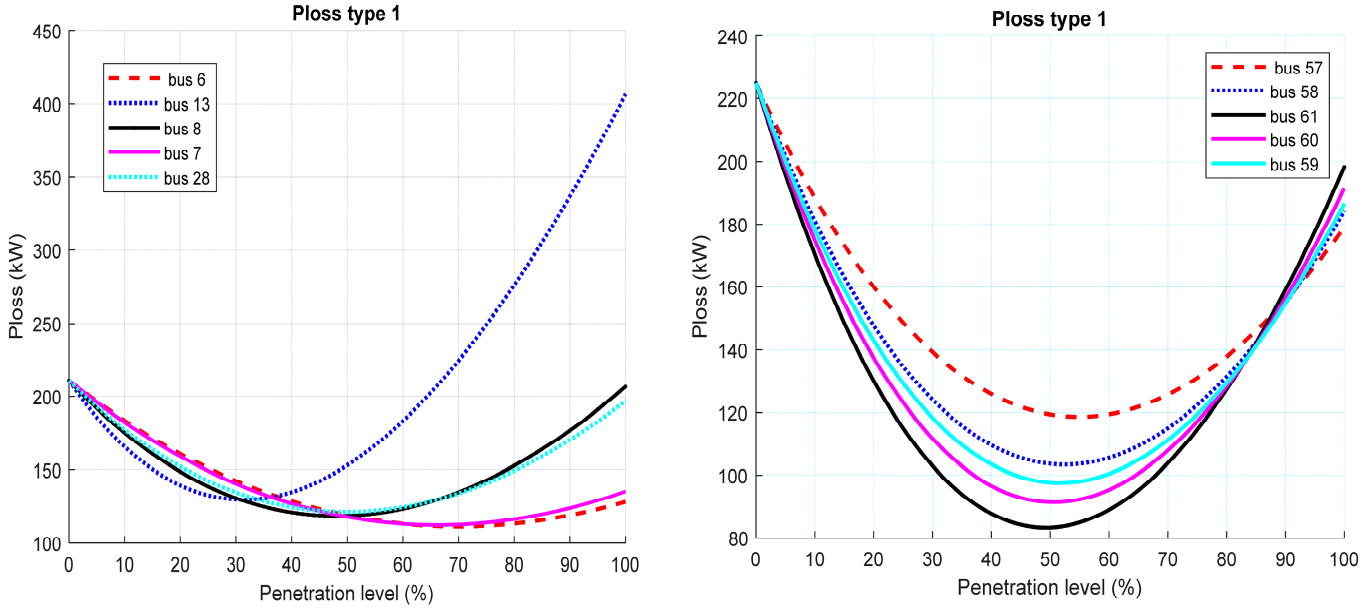

Figure 13. Real power loss when Type 1 DG was interconnected to selected nodes of (**a**) IEEE 33-bus (**b**) IEEE 69-bus.

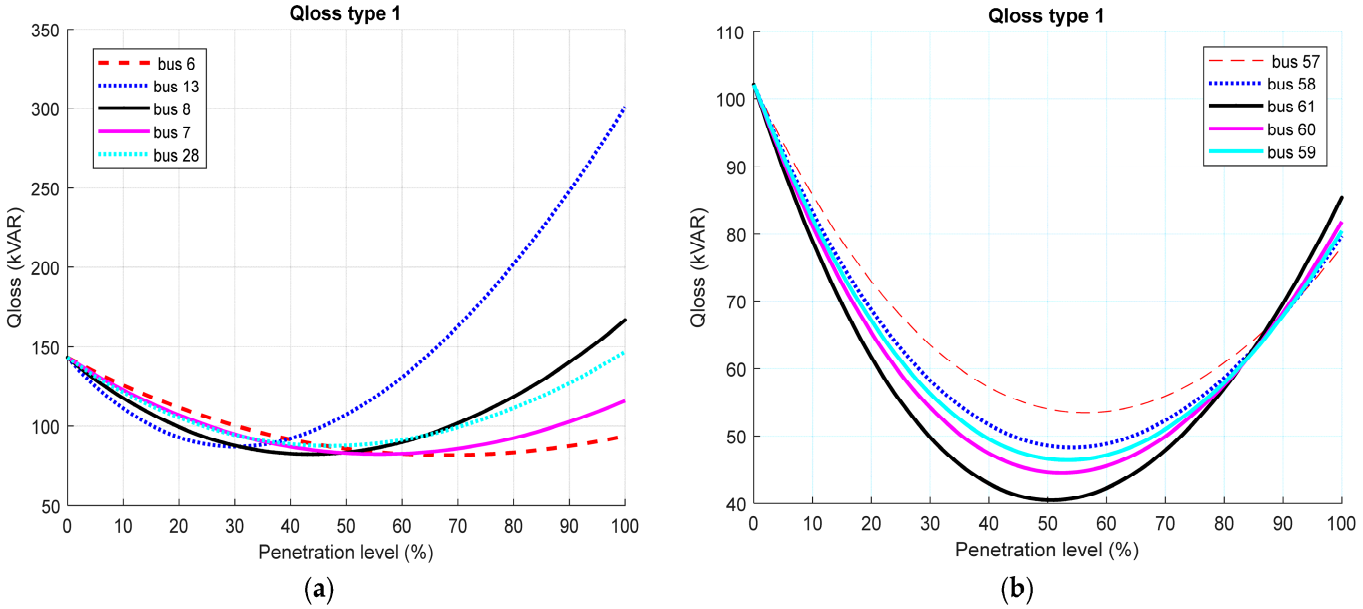

Figure 14. Reactive power loss when Type 1 DG was interconnected to selected nodes of IEEE (**a**) 33-bus (**b**) 69-bus RDNs.

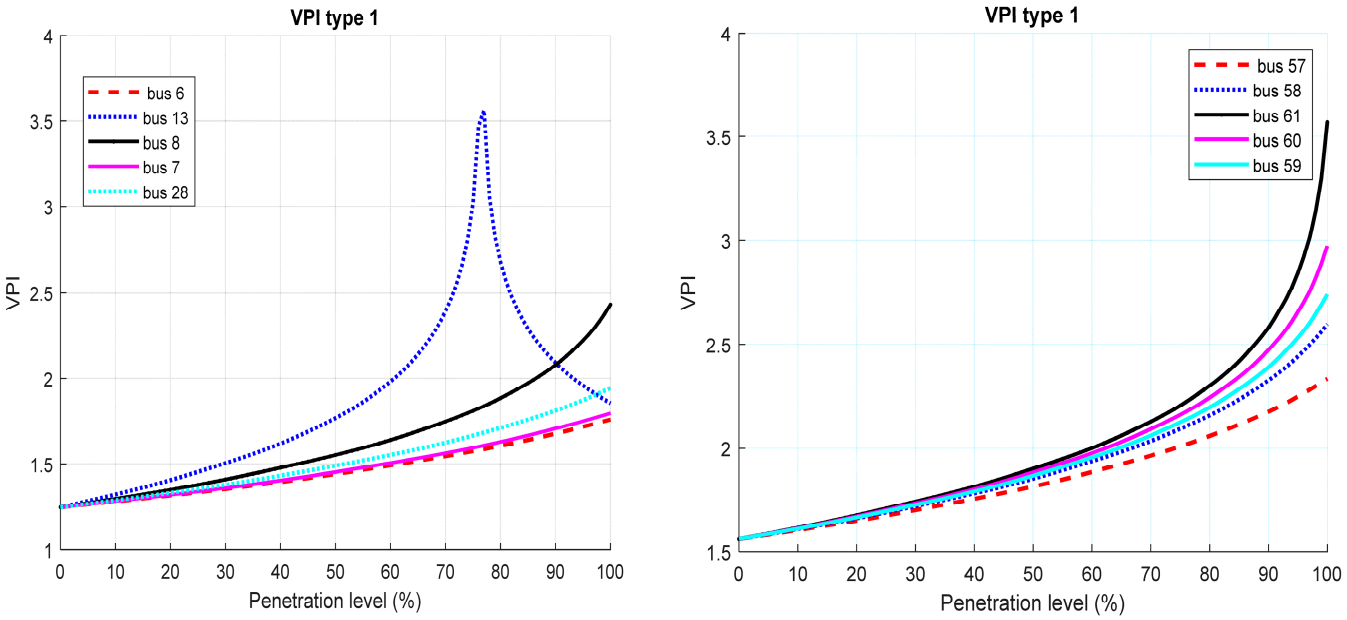

Figure 15. VPI when Type 1 DG was connected to selected buses of IEEE (**a**) 33-bus (**b**) 69-bus RDNs.

As the Type 1 DG penetration level grew, it was shown from Figures 13 and 14 that the real and reactive power losses had a quadratic property with a minimum value. This shows that the network's use of DG has a good impact on reducing overall real and reactive power losses during the initial penetration (when Type 1 DG was low). However, the real and reactive power losses began to rise as the penetration level rose over a certain threshold, suggesting that with greater Type 1 DG penetration levels than a certain least point, the real and reactive power losses rise. The data also show that there is a least penetration level (PL_{min}) where real and reactive losses are the smallest. Nevertheless, this point varies from bus to bus. These points occur at 70%, 28%, 45%, 62%, and 46% for both the real and reactive power losses for the 33-bus system while the corresponding points occur at 55%, 53%, 49%, 51%, and 55% penetration levels for the 69-bus network for the sensitive buses, respectively. At this point, the 33-bus network's real power losses in kW and reactive power losses in kVar were respectively 111.0, 130.3, 118.5, 112.4, and 121.5; and 81.7, 87.7, 82.4, 82.4, and 87.63; whereas the corresponding values for the 69-bus network were 118.6, 103.3, 83.19, 91.36, and 97.58; and 53.43, 48.30, 40.53, 44.51, and 46.42. It was also noted that the losses (active and reactive power) were the least at buses 6 and 61 for the 33-bus and 69-bus distribution networks, respectively. The VPI, as shown in Figure 15, demonstrates a clear correlation between the VPI and penetration level since the penetration of Type 1 DG improves the voltage profile continuously when compared to the base case scenario for the two networks. The increase in VPI implies that the magnitudes of the bus voltages are approaching the ideal voltage (the magnitude of the ideal voltage is taken as one) with increase in the penetration level of DG. The only exception was bus 13 for the 33-bus system where there was a continuous improvement until about 77% PL before the VPI began to decrease.

6.3. Impact of Type 2 DG on the Radial Distribution Network

The Type 1 DG was replaced with the type 2 DG and the impact of increasing its penetration level on the technical parameters being considered was again studied. The results are depicted in Figures 16–18.

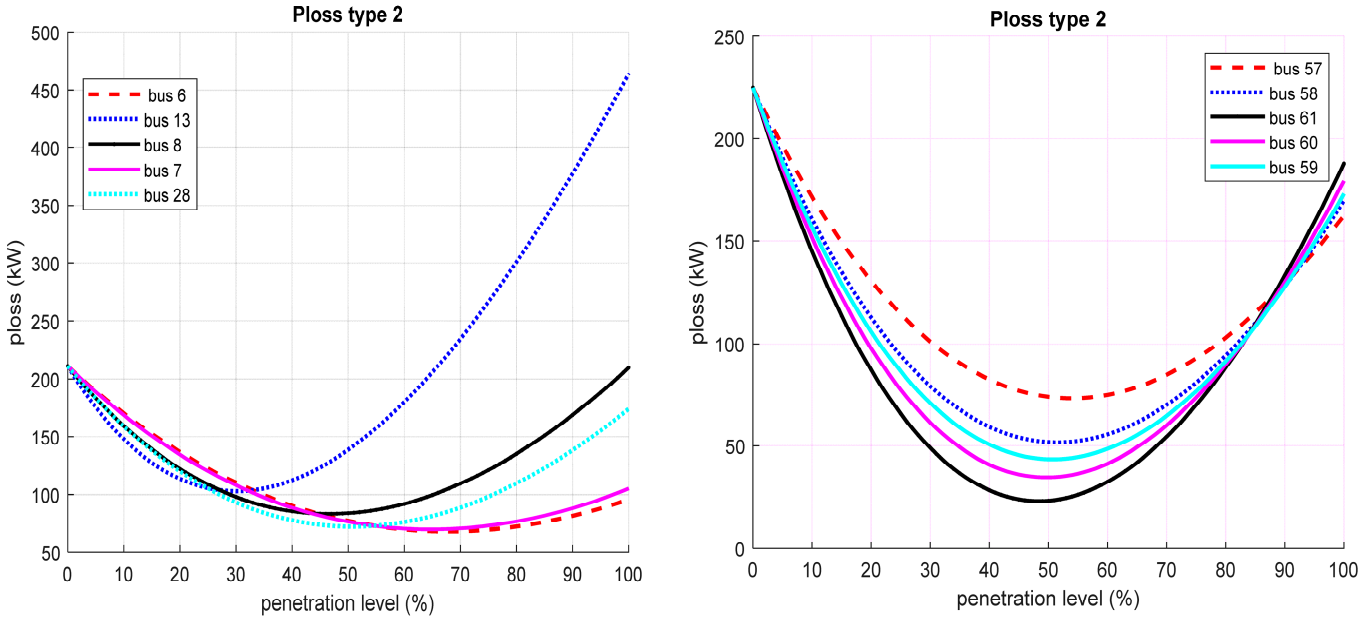

(**a**) (**b**)

Figure 16. Real power loss when Type 2 DG was connected to selected buses of IEEE (**a**) 33-bus (**b**) 69-bus RDNs.

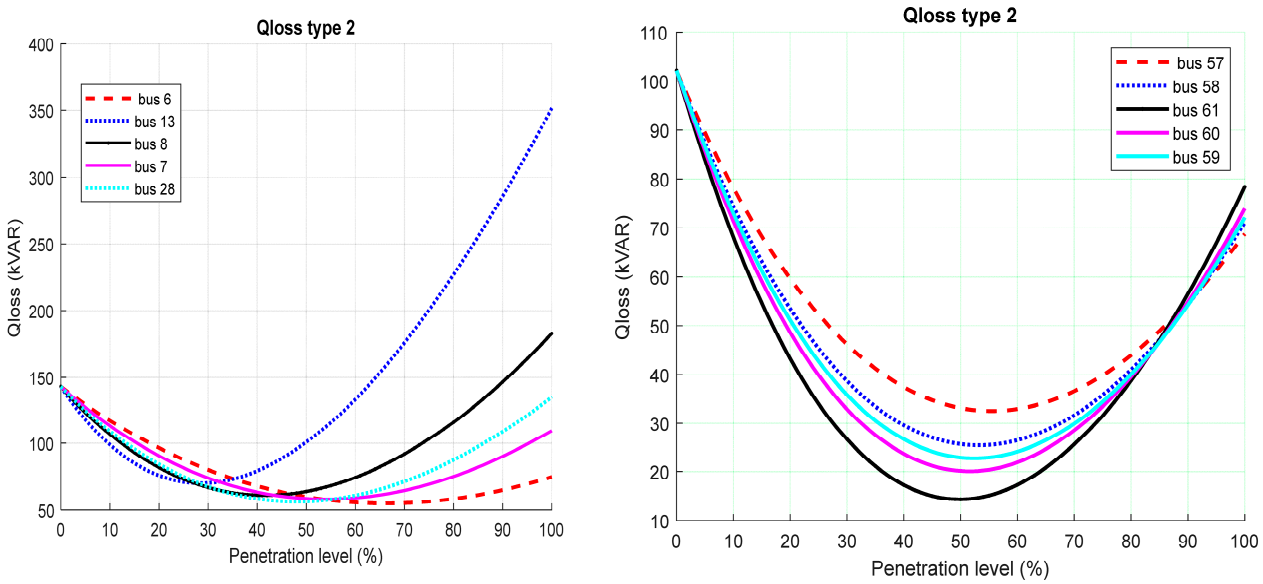

(**a**) (**b**)

Figure 17. Reactive power loss when Type 2 DG was interconnected to selected nodes of IEEE (**a**) 33-bus (**b**) 69-bus RDNs.

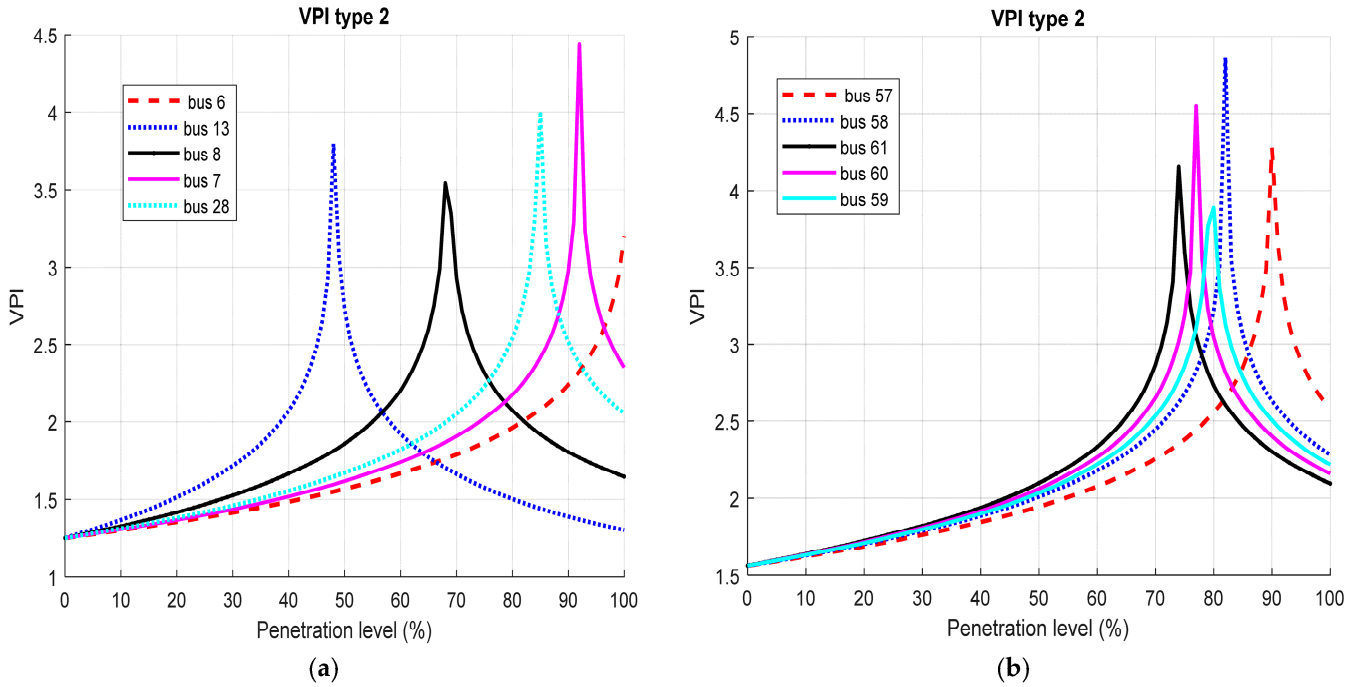

Figure 18. VPI when Type 2 DG was connected to the selected buses of IEEE (**a**) 33-bus (**b**) 69-bus RDNs.

From Figures 16 and 17, it is noted that the two curves of the real and reactive power losses exhibit the quadratic shape with minimum value in a similar fashion to Type 1 DG. This denotes that there was a continuous reduction of the losses with an increase in penetration level (PL) until a point of minimum power loss was reached (PL_{min}) beyond which the losses begin to increase. These thresholds occur for the IEEE 33-bus network at 67, 28, 45, 62, and 46% PL for real and reactive losses, respectively. For the IEEE 69 bus system, the analogous points occur at 55, 53, 49, 51, and 51% penetration levels. At these points, the real power losses in kW and reactive power losses in kVar for the IEEE 33-bus network were 67.94, 97.72, 81.62, 70.62, and 72.14; and 54.84, 70.16, 60.13, 59.34, and 56.13, respectively. The real power and reactive losses for the IEEE 69-bus system were 73.38, 51.78, 23.16, 34.65, and 43.53; and 32.60, 25.45, 14.31, 20.06, and 22.72, respectively. It was once again mentioned that for the IEEE 33 and IEEE 69-bus networks, respectively, buses 6 and 61 had the lowest losses (active and reactive power). The VPI, as shown in Figure 18, demonstrates a direct correlation between the VPI and penetration level because the voltage profile continuously improved as Type 2 DG was introduced compared to the base case scenario up to a certain penetration level, after which the VPI started to decline for all the buses taken into consideration for the two distribution networks.

6.4. Impact of Type 3 DG on the Radial Distribution Network

A Type 3 DG was used in place of the Type 2 DG, and simulations were run for both networks. Figures 19–21 provide the findings that show how the DG affects real power and reactive losses as well as the voltage profile.

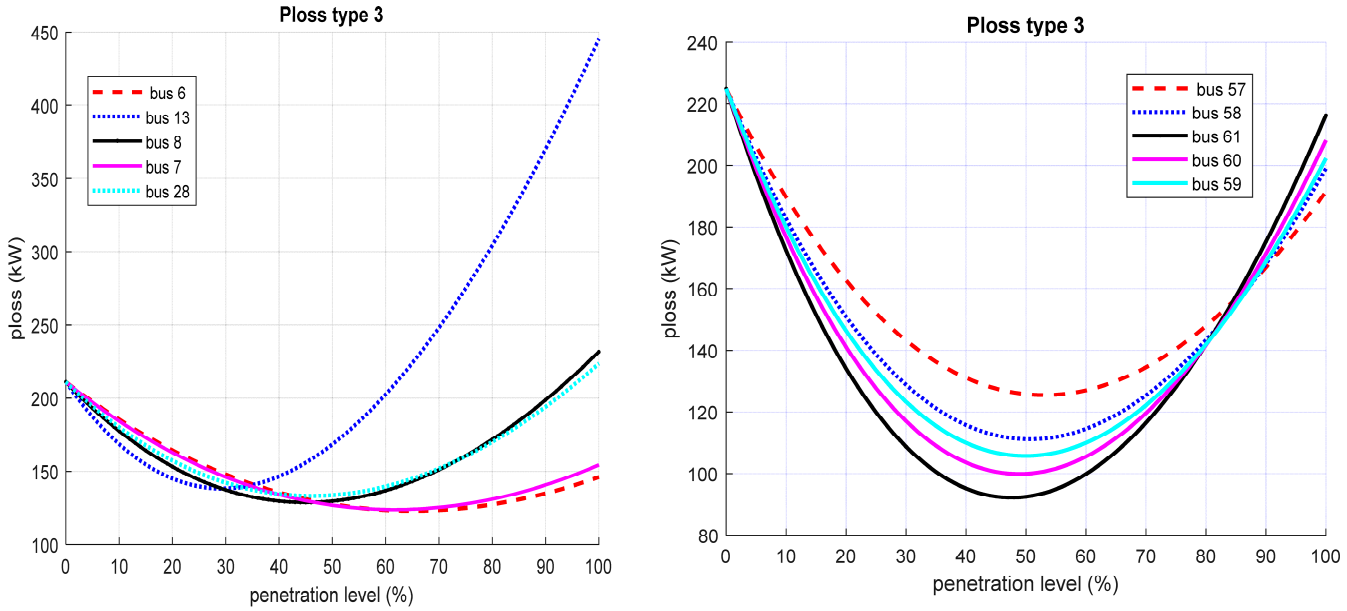

Figure 19. Real power loss when Type 3 DG was connected to selected buses of IEEE (**a**) 33-bus (**b**) 69-bus RDNs.

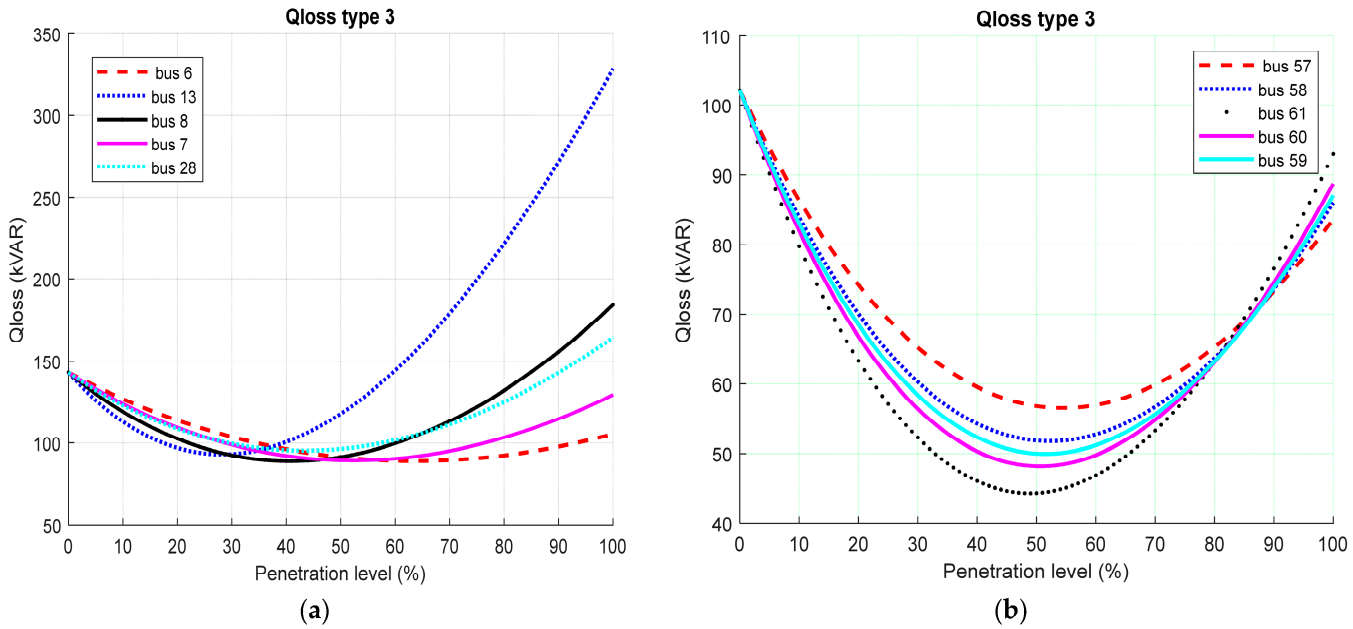

Figure 20. Reactive power loss when Type 3 DG was interconnected to selected nodes of IEEE (**a**) 33-bus (**b**) 69-bus RDNs.

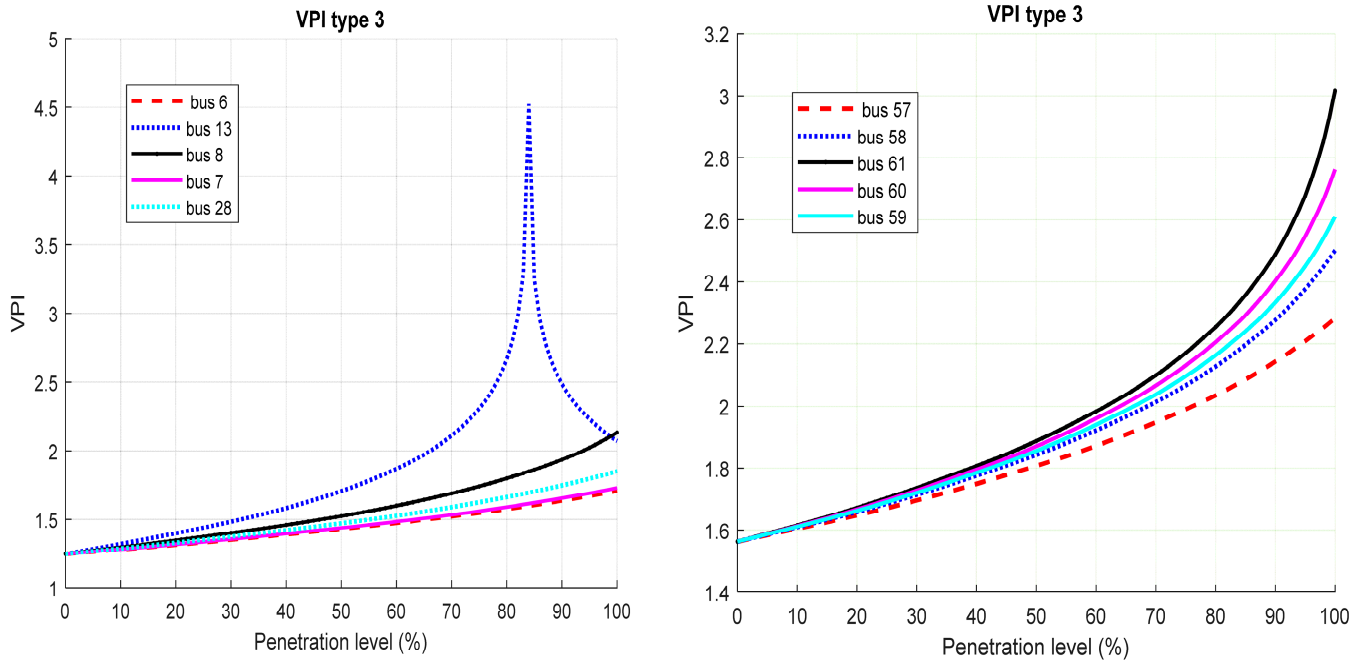

Figure 21. VPI when Type 3 DG was interconnected to the selected nodes of (**a**) 33-bus (**b**) 69-bus RDNs.

From Figures 19 and 20, it was observed that the connection of Type 3 to the network resulted in a reduction of the real and reactive losses at the smaller penetration level up to the maximum penetration level (PL_{min}) above which the losses increase with increasing penetration level. According to the data, the least power loss on the IEEE 33-bus was attained at a penetration level of between 47 and 63%, whereas the smallest power loss on the IEEE 69-bus occurs at a penetration level of between 50 and 53%. It was once again noticed from Figures 18 and 19 that Bus 6 has the lowest real and reactive power losses for the IEEE 33-bus network, whereas Bus 61 has the lowest for the IEEE 69-bus network. Figure 21 shows that the network's VPI was greater than it was in the base case scenario, demonstrating that the voltage profile improved as the DG's penetration level increased. The only exception was bus 13 of the IEEE 33-bus system where there was a continuous improvement of the VPI until 82% PL before for the VPI begins to drop.

6.5. Impact of Type 4 DG on the Radial Distribution Network

Type 4 DG was then connected to the system after the removal of Type 3 DG and simulation was performed to determine its impact on the real and reactive power losses, and the network voltage profile. The results are displayed in Figures 22–24.

Figures 22 and 23 showed that the real and reactive power losses decreased when Type 4 DG was interconnected to the system at lower penetration levels up to the peak penetration level, after which the losses increased with increasing penetration level (PL_{min}). The PL_{min} occurs between 53 and 76% PL on the IEEE 33-bus network, but between 50 and 55% PL on the IEEE 69-bus network. It was once again mentioned that for the IEEE 33 and IEEE 69-bus networks, respectively, buses 30 and 61 had the lowest losses. Figure 24 indicates that the network's VPI was greater than the base scenario, demonstrating that the voltage profile significantly and continuously improved with rising Type 4 DG penetration levels.

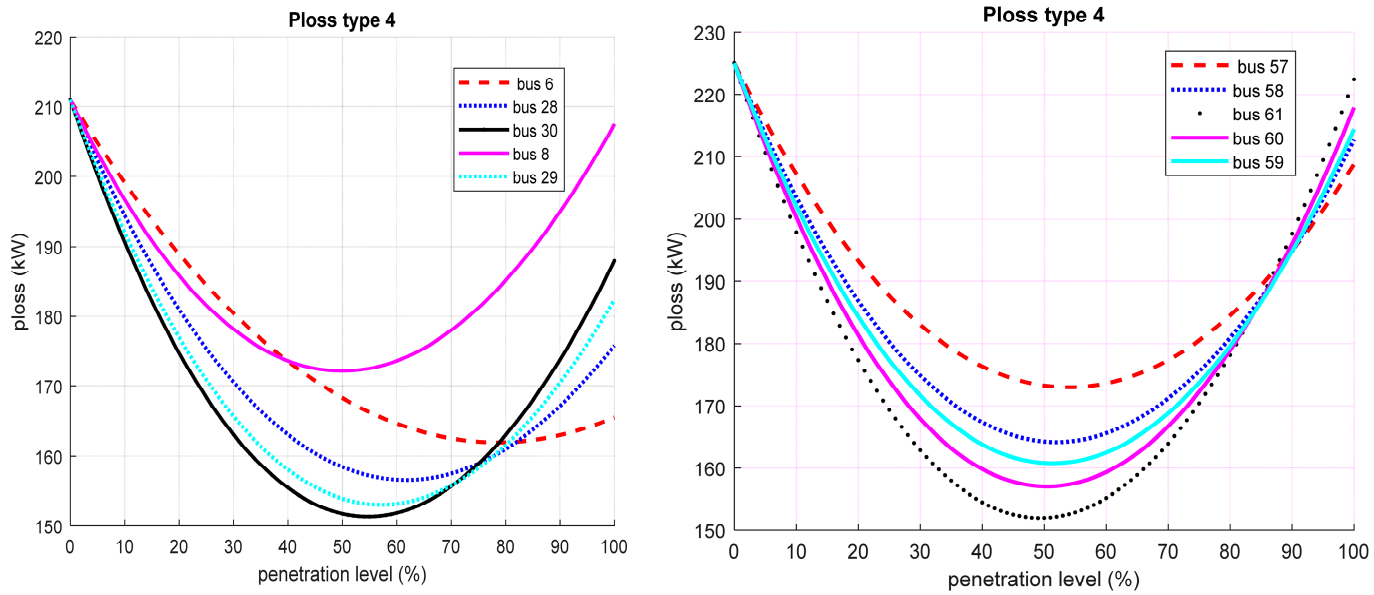

Figure 22. Real power loss when Type 4 DG was interconnected to selected nodes of the IEEE (**a**) 33-bus (**b**) 69 bus RDNs.

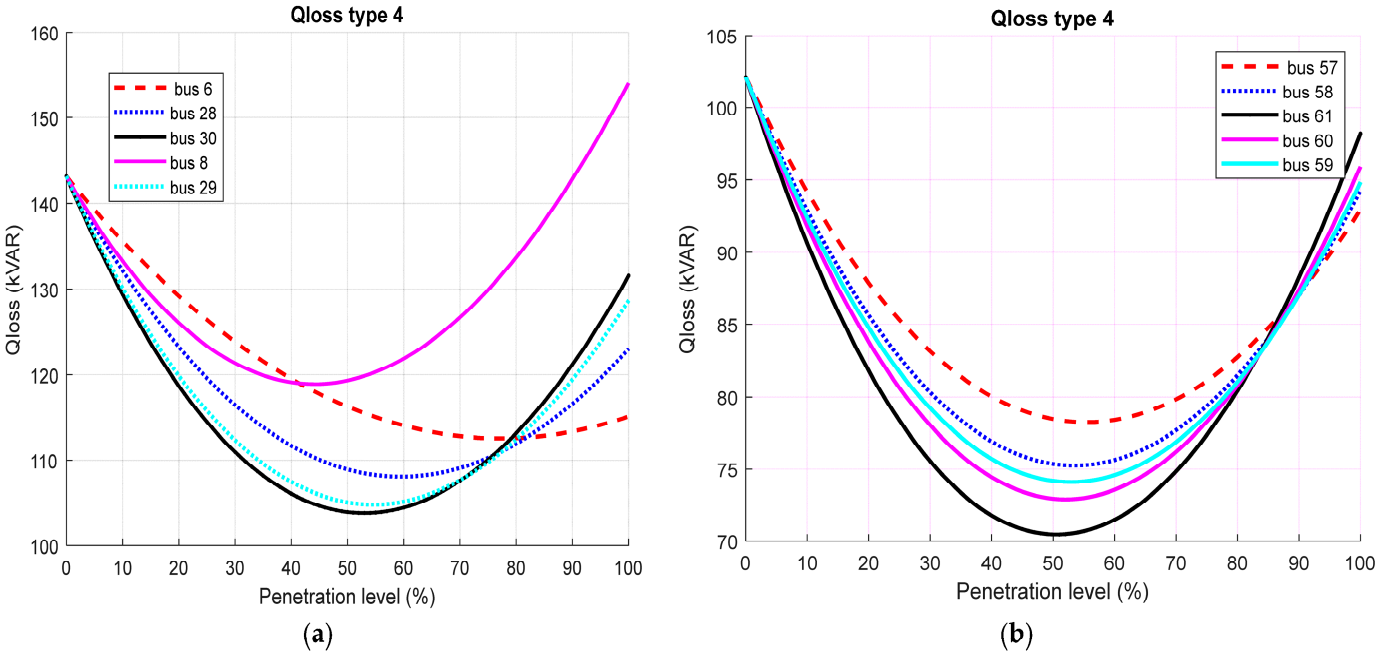

Figure 23. Qloss when Type 4 DG was interconnected to the selected nodes of IEEE (**a**) 33-bus (**b**) 69-bus RDNs.

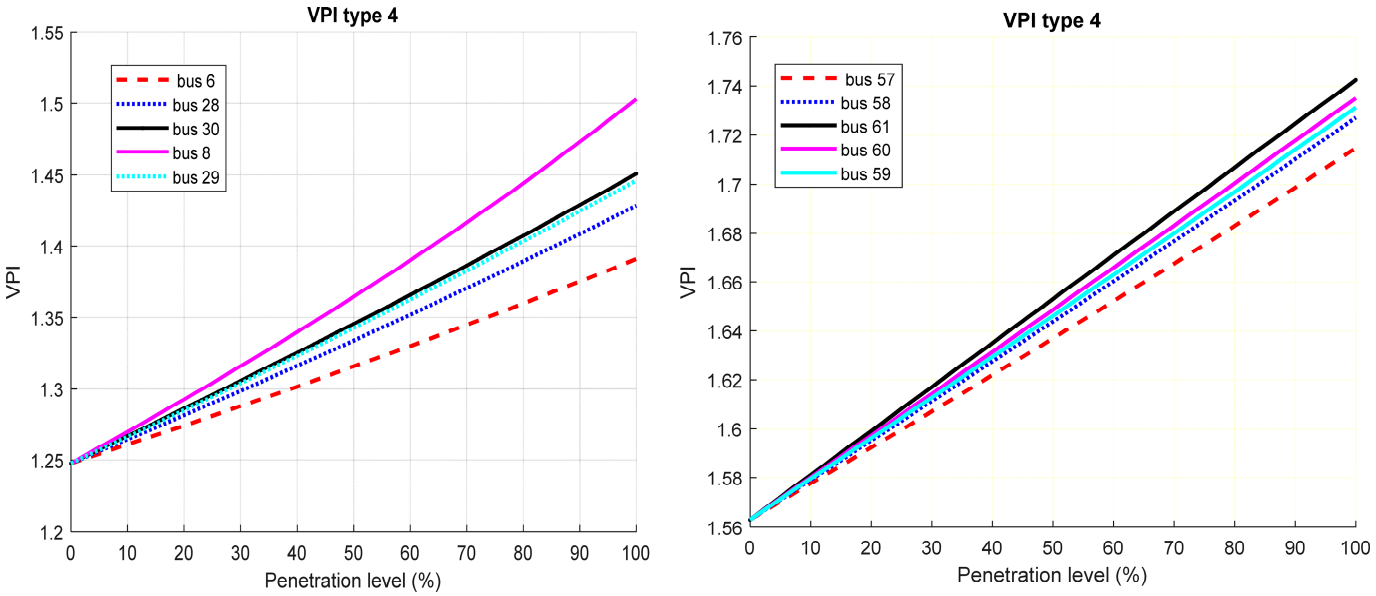

Figure 24. VPI when Type 4 DG was interconnected to the selected nodes of IEEE (**a**) 33-bus (**b**) 69-bus RDNs.

6.6. Compparison of the DG Types

With each DG type interconnected to buses 6 and 61 for the IEEE 33 and IEEE 69-bus networks, respectively, simulation was run to gain insight into the potential effects of the various DG types on the distribution networks. For real and reactive power loss, as well as the VPI, the findings are illustrated in Figures 25–27, respectively.

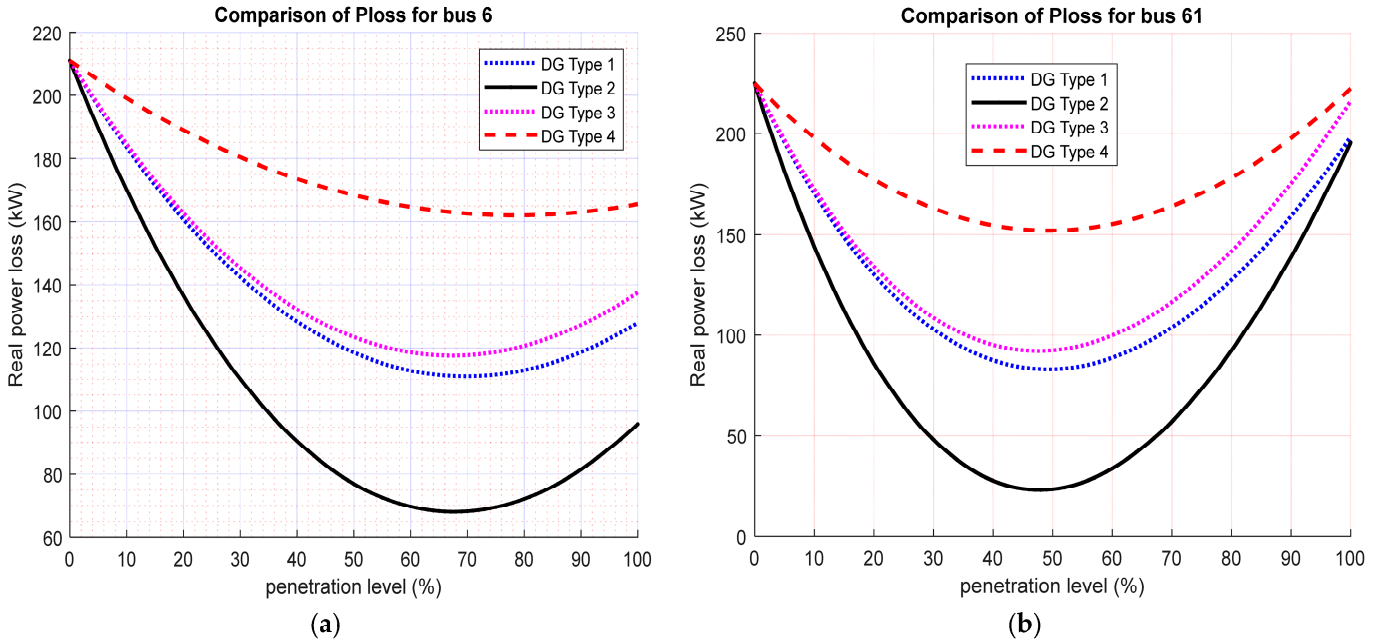

Figure 25. Comparison of real power loss by various DG types interconnected to (**a**) bus 6 of IEEE 33-bus and (**b**) bus 61 of the IEEE 69-bus RDNs.

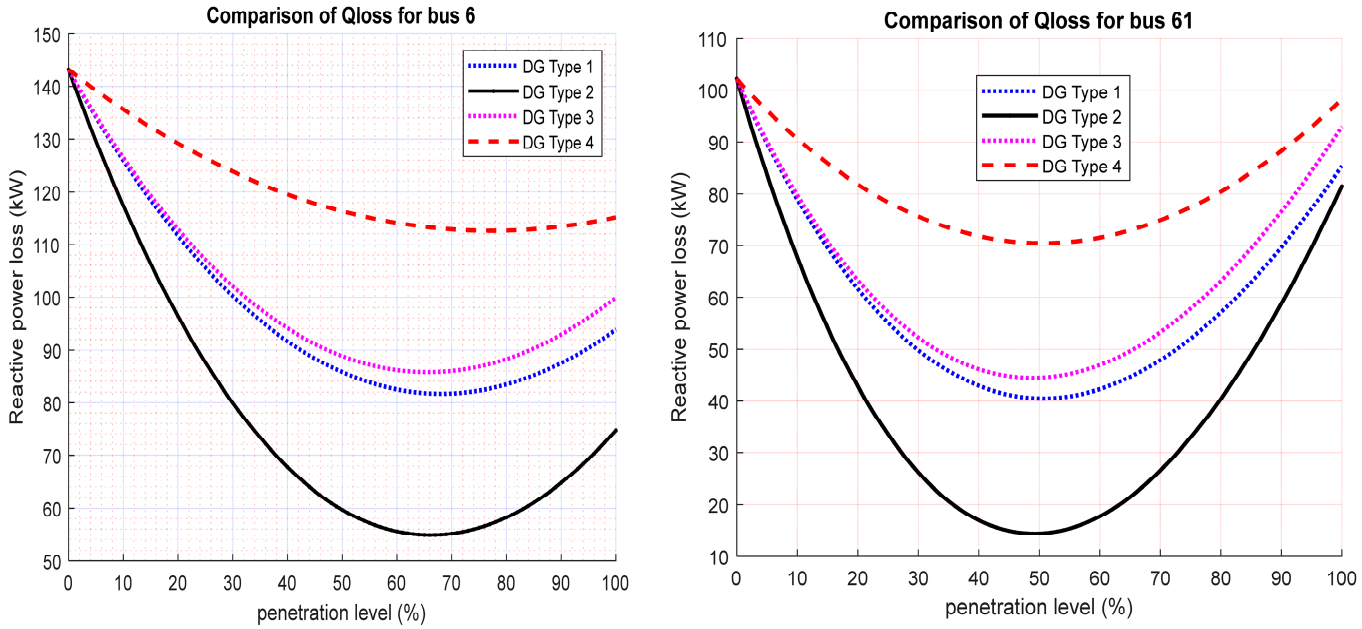

Figure 26. Comparison of reactive power loss by different DG types interconnected to (**a**) bus 6 of IEEE 33-bus and (**b**) bus 61 of the IEEE 69-bus RDNs.

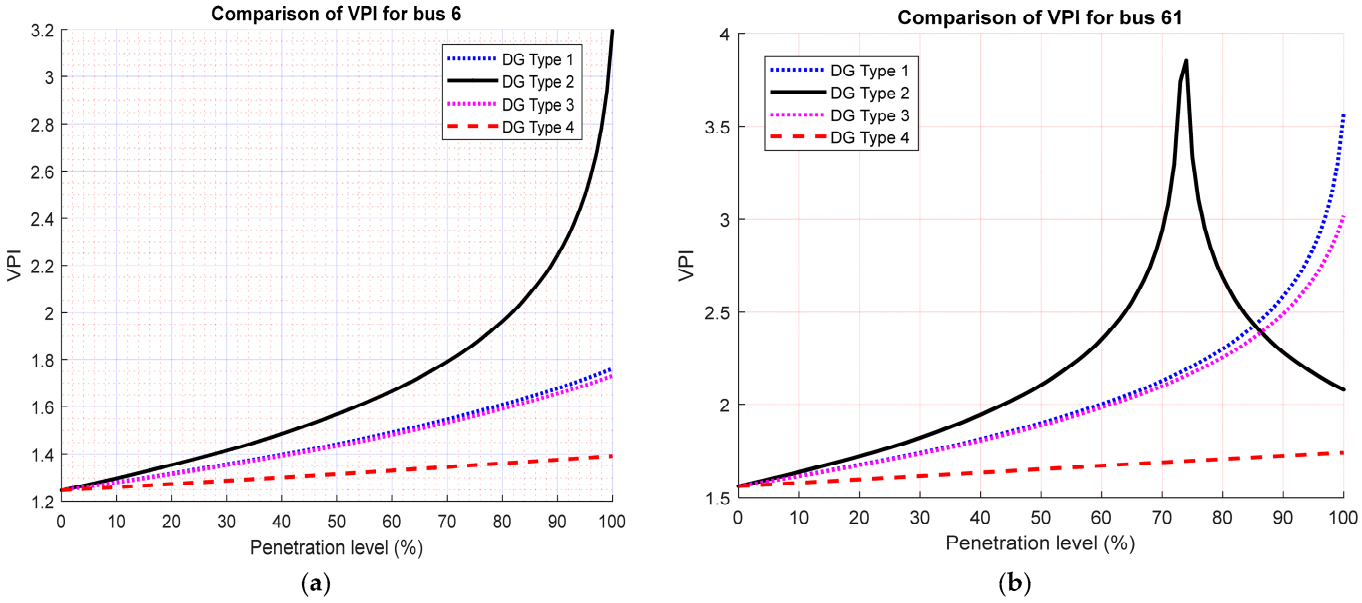

Figure 27. Comparison of VPI by various DG types interconnected to (**a**) bus 6 of IEEE 33-bus and (**b**) bus 61 of the IEEE 69-bus network.

In summary, Figures 25 and 26 show that DG integration into the distribution network may decrease real and reactive power losses. The data showed that the Type 2 DG performed better than the other DG types, with real and reactive power losses being lower with the Type 2 DG than with the other three DG types. This was followed by the Type 1 DG, and Type 3 DG while the Type 4 DG has the least performance. This was because Type 4 DG has the ability of injecting only reactive power with no real power injection in comparison to the other DG Types. Figure 27 revealed that the Type 2 DG has the highest voltage profile index, showing that it performed better in comparison to other DG Types on the voltage

profile of the two networks. This was because Type 2 DG has the capability of supplying both real and reactive powers into the network.

The optimal location and size of the DG Types for minimum loss can be obtained from Figures 25 and 26. This may be used as a reference point to confirm the outcomes of the optimal values of the optimal allocation of a single DG allocation issue achieved by any optimization technique in the distribution network. For instance, the least PL_{min} of the Figures occurs at bus 61 for the IEEE 69-bus network for Type 1 DG. This was considered to be the optimal bus. The magnitude of the PL_{min} for the Type 1 DG was 49.0% which corresponds to 1863 kW. The real and reactive power losses at this point were 83.19 kW and 43 kVar. The PL_{min}, DG size, optimal bus, and the corresponding losses for all the DG types for the two networks are shown in Table 6. The optimum results obtained from the penetration of the DG types were used to confirm the results of recent techniques utilized for the optimum allocation problem of single DG types on the IEEE 33 and 69-bus systems in Tables 7 and 8 respectively for DG Types 1, 2 and 4. The results of Type 3 DG were not included in the comparison Table due to paucity of literatures on optimal allocation of Type 3 DG. The proposed approach gave a better percentage power loss reduction (%Ploss) in most of the DG type scenarios compared to other existing studies for both the IEEE 33 and 69-bus RDNs.

Table 6. Optimal allocations deduced for the DG Types.

	IEEE 33-Bus RDN				**IEEE 69-Bus RDN**			
	Type 1 DG	**Type 2 DG**	**Type 3 DG**	**Type 4 DG**	**Type 1 DG**	**Type 2 DG**	**Type 3 DG**	**Type 4 DG**
PL_{min}(%)	70.0	67	63	53	49.0	48.0	48.0	48.0
Size (kW)	2601	2489.1	2340.5	——	1863.0	1710.8	1825.0	——
Size (kVar)	——	1800	538.3	1219	——	1283.1	534.6	1293.1
Optimal bus	6	6	6	30	61	61	61	61
Ploss (kW)	111.00	67.94	124.0	151.4	83.19	23.16	92.21	152.1
Qloss (kVar)	81.70	54.84	89.19	103.9	40.52	14.31	70.49	51.60
% Ploss	47.39	67.80	41.23	28.25	63.03	89.71	59.01	32.40
% Qloss	42.87	61.65	43.22	27.34	60.31	85.99	30.9	49.48

Table 7. Comparative Study for the optimal results for the 33-bus network.

DG Type	**Author (year)**	**Technique**	**Bus**	**Size**	**Ploss (kW)**	**Qloss (kVar)**	**%Ploss**
BC		———	—-	———	211	143	———
Type 1 DG(kW)	Hassan et al. (2015) [50]	GA	6	2380	132.64	N.A.	37.14
	Kansal et al. (2016) [51]	Hybrid	6	2490	111.17	N.A.	47.31
	Sudabattula and kowsalya (2016) [52]	FPA	6	2300	112.2	N.A.	46.82
	Prakash and Lakshminarayana (2018) [53]	WOA	6	2589.6	111.00	81.69	47.39
	El-fergany (2015) [54]	BSOA	8	1857.5	118.10	N.A.	44.03
	Kashyap et al. (2022) [55]	Analytical	6	2491	111.10	N.A.	47.35
	Proposed method		6	2601	111.00	81.70	47.39
Type 2 DG (kVA)	Hassan et al. (2015) [50]	GA	6	2980	72.68	N.A.	64.32
	El-fergany (2015) [54]	BSOA	8	2265.2	82.78	N.A.	60.76
	Reddy et al. (2017) [22]	WOA	15	1061	133.50	41.88	
	Prakash and Lakshminarayana (2018) [53]	WOA	6	2557.6	67.86	54.83	67.84
	Ali et al. (2017) [23]	ALO	6	2238.8	71.75	N.A.	65.99
	Kashyap et al. (2022) [55]	Analytical	6	3028	68.0	N.A.	67.77
	Proposed method		6	3071.7	67.94	61.65	67.80
Type 4 (kVAr)	Salimon et al. (2020) [56]	CSA	30	1200	151.52	103.4	28.18
	Okelola et al. (2022) [57]	WOA	30	1259	151.40	104.0	28.25
	Kashyap et al. (2022) [55]	Analytical	30	1230	151.40	N.A.	28.25
	Proposed method		30	1219	151.40	151.4	28.25

Table 8. Comparative Study for the optimum results for IEEE 69-bus network.

DG Type	Author (year)	Technique	Bus	Size	Ploss (kW)	Qloss (kVar)	%Ploss
Base case		———	——	———	224.96	102.14	———
Type 1(kW)	Hassan et al. (2015) [50]	GA	61	1872.0	83.19	N.A.	63.02
	Abdelaziz et al. (2015) [58]	BB-BC	61	1872.5	83.22	N.A.	63.01
	Kansal et al. (2016) [51]	Hybrid	61	1800.0	62.95	N.A.	62.95
	Reddy et al. (2017) [22]	WOA	61	1872.8	83.23	N.A.	63.01
	Ali et al. (2017) [23]	ALO	61	1800.0	83.38	N.A.	62.94
	Prakash and Lakshmina-rayana (2018) [53]	WOA	61	1856.1	83.20	40.54	63.02
	Mahmoud et al. (2016) [59]	EA	61	1878.0	83.23	N.A.	63.00
	Mohammed et al. (2021) [60]	Hybrid	61	1810.0	83.37	N.A.	62.95
	Elseify et al. (2022) [61]	HBA	61	1872.7	83.22	N.A.	63.01
	Kashyap et al. (2022) [55]	Analytical	61	1810.0	83.30	N.A.	62.98
	Proposed method		61	1863.0	83.19	40.52	63.03
Type 2(kVA)	Hassan et al. (2015) [50]	GA	61	2155.6	38.46	N.A.	82.90
	Abdelaziz et al. (2015) [58]	BB-BC	61	2223.0	23.17	N.A.	89.70
	Reddy et al. (2017) [22]	WOA	61	2217.4	27.96	16.46	87.57
	Ali et al. (2017) [23]	ALO	61	2227.9	23.16	N.A.	89.70
	Prakash and Lakshmina-rayana (2018) [53]	WOA	61	2305.1	23.16	14.38	89.70
	Kansal et al. (2016) [51]	Hybrid	61	2240.0	23.19	N.A.	89.67
	Nowdeh et al. (2019) [62]	TLBO-GWO	61	1000.0	58.8	N.A.	73.86
	Mahmoud et al. (2016) [59]	EA-OPF	61	1828.0	23.17	N.A.	89.70
	Elseify et al. (2022) [61]	HBA	61	1828.5	23.17	N.A.	89.70
	Kashyap et al. (2022) [55]	Analytical	61	2222.0	23.17	N.A.	89.70
	Proposed method		61	2138.5	23.16	14.31	89.71
Type 4 (kVAr)	Kansal et al. (2016) [51]	Hybrid	61	1290.0	152.10	N.A.	32.40
	Reddy et al. (2017) [22]	WOA	61	1330.0	152.06	70.51	32.42
	Kashyap et al. (2022) [55]	Analytical	61	1290.0	152.1	N.A.	52.31
	Proposed method		61	1293.1	152.1	51.6	52.31

7. Conclusions

On the most delicate buses in the distribution networks, the impacts of the penetration levels of the four DG types on real and reactive losses as well as the voltage profile were examined. The sensitive buses of the distribution network were selected using a novel effective power voltage stability index, EPVSI and EQVSI. The results lead to the following conclusion:

1. The proposed EPVSI bus ranking approach based on effective power can effectively identify the weakest or sensitive buses for distributed generation and EQVSI for capacitor penetration.
2. In general, all types of DG lower power losses in a distribution system. For the sensitive buses that were the subject of the investigation, the degree of the loss reduction differs for different DG types.
3. With a rise in their penetration level, DG types' effects on power losses formed a minimum quadratic characteristic curve, suggesting that losses are reduced at low penetration levels. However, once the amount of DG penetration is raised past a certain point, power losses begin to rise. This suggests that there is a maximum penetration level at which DG causes increased power losses in the system.
4. The amount of penetration needed to achieve the lowest loss varies depending on the connected DG type and bus to bus.
5. The VPI is generally directly proportional to the DG penetration level for most of the DG types.

6. In terms of power loss and voltage profile of the distribution networks with the lowest power loss and highest VPI, the Type 2 DG performs best. Since the DG type may provide reactive as well as real power to the RDN, this is to be expected. Due to its inability to provide the network with real power, the Type 4 DG performs the worst.
7. The deduced results obtained from the analytical penetration level of DG may be used as a benchmark to validate the optimal results obtained for DG and capacitor placement and sizing from optimization techniques.

A single-distributed generator (DG) penetration was considered in this study. Future research can consider how the degree of penetration of multiple DGs simultaneously could affect the distribution network's power losses and voltage profile.

Author Contributions: Conceptualization, S.A.S.; methodology, S.A.S.; software, S.A.S.; validation, G.A.A., I.G.A., S.O.A., H.O.R.H. and O.B.A.; investigation, S.A.S. and O.B.A.; data curation, S.A.S., I.G.A. and S.O.A., resources, H.O.R.H. and O.B.A.; writing—original draft preparation, S.A.S.; writing—review and editing, G.A.A., I.G.A., S.O.A. and S.A.S.; supervision, G.A.A. and I.G.A.; project administration, G.A.A. and I.G.A. All authors have read and agreed to the published version of the manuscript.

Funding: This research received no external funding.

Data Availability Statement: Not applicable.

Conflicts of Interest: The authors declare no conflict of interest.

References

1. Ayanlade, S.O.; Komolafe, O.A. Distribution system voltage profile improvement based on network structural characteristics. In Proceedings of the OAU Faculty of Technology Conference 2019 (OAUTEKConF 2019), OAU, Ile-Ife, Osun State, Nigeria, 22–25 September 2019; pp. 75–80.
2. Mokryani, G. Distribution network types and configurations. In *Future Distribution Networks: Planning, Operation, and Control*; AIP Publishing LLC: Melville, NY, USA, 2022; p. 1.
3. Okelola, M.O.; Salimon, S.A.; Adegbola, O.A.; Ogunwole, E.I.; Ayanlade, S.O.; Aderemi, B.A. Optimal siting and sizing of D-STATCOM in distribution system using new voltage stability index and bat algorithm. In Proceedings of the 2021 International Congress of Advanced Technology and Engineering (ICOTEN), Taiz, Yemen, 4–5 July 2021; IEEE: Toulouse, France; pp. 1–5.
4. Camilo, F.M.; Almeida, M.E.; Castro, R.; Pires, V.F. Multi-conductor line models for harmonic load-flow calculations in LV networks with high penetration of PV generation. *J. Mod. Power Syst. Clean Energy* **2021**, *10*, 1288–1301. [CrossRef]
5. Salimon, S.A.; Lawal, Q.O.; Adebiyi, O.W.; Okelola, M.O. Cost-Benefit of Optimal Allocation of DSTATCOM in Distribution Networks Using Ant-Lion Optimization Algorithm. *Period. Polytech. Electr. Eng. Comput. Sci.* **2022**, *66*, 350–360. [CrossRef]
6. Iweh, C.D.; Gyamfi, S.; Tanyi, E.; Effah-Donyina, E. Distributed generation and renewable energy integration into the grid: Prerequisites, push factors, practical options, issues and merits. *Energies* **2021**, *14*, 5375. [CrossRef]
7. Adefarati, T.; Bansal, R.C. Integration of renewable distributed generators into the distribution system: A review. *IET Renew. Power Gener.* **2016**, *10*, 873–884. [CrossRef]
8. Bajaj, M.; Singh, A.K. Grid integrated renewable DG systems: A review of power quality challenges and state-of-the-art mitigation techniques. *Int. J. Energy Res.* **2020**, *44*, 26–69. [CrossRef]
9. Ismael, S.M.; Aleem, S.H.; Abdelaziz, A.Y.; Zobaa, A.F. State-of-the-art of hosting capacity in modern power systems with distributed generation. *Renew. Energy* **2019**, *130*, 1002–1020. [CrossRef]
10. Chandran, C.V.; Basu, M.; Sunderland, K.; Pukhrem, S.; Catalao, J.P. Application of demand response to improve voltage regulation with high DG penetration. *Electr. Power Syst. Res.* **2020**, *189*, 106722. [CrossRef]
11. Iqbal, F.; Khan, M.T.; Siddiqui, A.S. Optimal placement of DG and DSTATCOM for loss reduction and voltage profile improvement. *Alex. Eng. J.* **2018**, *57*, 755–765. [CrossRef]
12. Ayodele, T.R.; Ogunjuyigbe, A.S.; Akinola, O.O. Optimal location, sizing, and appropriate technology selection of distributed generators for minimizing power loss using genetic algorithm. *J. Renew. Energy* **2015**, *2015*, 832917. [CrossRef]
13. Veerasamy, V.; Wahab, N.I.; Ramachandran, R.; Othman, M.L.; Hizam, H.; Devendran, V.S.; Irudayaraj, A.X.; Vinayagam, A. Recurrent network based power flow solution for voltage stability assessment and improvement with distributed energy sources. *Appl. Energy* **2021**, *302*, 117524. [CrossRef]
14. Xu, X.; Niu, D.; Peng, L.; Zheng, S.; Qiu, J. Hierarchical multi-objective optimal planning model of active distribution network considering distributed generation and demand-side response. *Sustain. Energy Technol. Assess.* **2022**, *53*, 102438. [CrossRef]
15. Hosseinzadeh, N.; Aziz, A.; Mahmud, A.; Gargoom, A.; Rabbani, M. Voltage stability of power systems with renewable-energy inverter-based generators: A review. *Electronics* **2021**, *10*, 115. [CrossRef]

16. Salimon, S.A.; Adepoju, G.A.; Adebayo, I.G.; Adewuyi, O.B.; Amuda, S.O. Simultaneous Placement and Sizing of Distributed Generation Units and Shunt Capacitors on Radial Distribution Systems using Cuckoo Search Algorithm. *Curr. J. Appl. Sci. Technol.* **2021**, *40*, 43–58. [CrossRef]
17. Adepoju, G.A.; Aderemi, B.A.; Salimon, S.A.; Alabi, O.J. Optimal Placement and Sizing of Distributed Generation for Power Loss Minimization in Distribution Network using Particle Swarm Optimization Technique. *Eur. J. Eng. Technol. Res.* **2023**, *8*, 19–25. [CrossRef]
18. Ali, M.H.; Salawudeen, A.T.; Kamel, S.; Salau, H.B.; Habil, M.; Shouran, M. Single-and multi-objective modified aquila optimizer for optimal multiple renewable energy resources in distribution network. *Mathematics* **2022**, *10*, 2129. [CrossRef]
19. Ali, M.H.; Kamel, S.; Hassan, M.H.; Tostado-Véliz, M.; Zawbaa, H.M. An improved wild horse optimization algorithm for reliability based optimal DG planning of radial distribution networks. *Energy Rep.* **2022**, *8*, 582–604. [CrossRef]
20. Dharavat, N.; Sudabattula, S.K.; Velamuri, S.; Mishra, S.; Sharma, N.K.; Bajaj, M.; Elgamli, E.; Shouran, M.; Kamel, S. Optimal allocation of renewable distributed generators and electric vehicles in a distribution system using the political optimization algorithm. *Energies* **2022**, *15*, 6698. [CrossRef]
21. Khan, M.H.; Ulasyar, A.; Khattak, A.; Zad, H.S.; Alsharef, M.; Alahmadi, A.A.; Ullah, N. Optimal Sizing and Allocation of Distributed Generation in the Radial Power Distribution System Using Honey Badger Algorithm. *Energies* **2022**, *15*, 5891. [CrossRef]
22. Reddy, P.D.P.; Reddy, V.C.V.; Manohar, T.G. Whale optimization algorithm for optimal sizing of renewable resources for loss reduction in distribution systems. *Renew. Wind. Water Sol.* **2017**, *4*, 3. [CrossRef]
23. Ali, E.S.; Abd Elazim, S.M.; Abdelaziz, A.Y. Ant Lion Optimization Algorithm for optimal location and sizing of renewable distributed generations. *Renew. Energy* **2017**, *101*, 1311–1324. [CrossRef]
24. Dash, S.K.; Mishra, S.; Abdelaziz, A.Y.; Alghaythi, M.L.; Allehyani, A. Optimal allocation of distributed generators in active distribution networks using a new oppositional hybrid sine cosine muted differential evolution algorithm. *Energies* **2022**, *15*, 2267. [CrossRef]
25. Beza, T.M.; Huang, Y.C.; Kuo, C.C. A hybrid optimization approach for power loss reduction and DG penetration level increment in electrical distribution network. *Energies* **2020**, *13*, 6008. [CrossRef]
26. Ogunjuyigbe, A.S.; Ayodele, T.R.; Akinola, O.O. Impact of distributed generators on the power loss and voltage profile of sub-transmission network. *J. Electr. Syst. Inf. Technol.* **2016**, *3*, 94–107. [CrossRef]
27. Şeker, A.A.; Gözel, T.; Hocaoğlu, M.H. An analytic approach to determine maximum penetration level of distributed generation considering power loss. In Proceedings of the 2018 Twentieth International Middle East Power Systems Conference (MEPCON), Cairo, Egypt, 18–20 December 2018; IEEE: Toulouse, France; pp. 956–961.
28. Kazeminejad, M.; Banejad, M.; Annakkage, U.D.; Hosseinzadeh, N. Load pattern-based voltage stability analysis in unbalanced distribution networks considering maximum penetration level of distributed generation. *IET Renew. Power Gener.* **2020**, *14*, 2517–2525. [CrossRef]
29. Duong, M.Q.; Tran, N.T.; Sava, G.N.; Scripcariu, M. The impacts of distributed generation penetration into the power system. In Proceedings of the 2017 International Conference on Electromechanical and Power Systems (SIELMEN), Iasi, Romania, 11–13 October 2017; IEEE: Toulouse, France; pp. 295–301.
30. Addurat, A.S.; Pasupuleti, J. The impacts of number of solar photovoltaic units on distribution network losses and voltage profile. In Proceedings of the 2020 IEEE Student Conference on Research and Development (SCOReD), Batu Pahat, Malaysia, 27–29 September 2020; IEEE: Toulouse, France; pp. 249–253.
31. Salimon, S.A.; Adepoju, G.A.; Adebayo, I.G.; Ayanlade, S.O. Impact of shunt capacitor penetration level in radial distribution system considering techno-economic benefits. *Niger. J. Technol. Dev.* **2022**, *19*, 101–109. [CrossRef]
32. Bokhari, A.; Raza, A.; Diaz-Aguilo, M.; de Leon, F.; Czarkowski, D.; Uosef, R.E.; Wang, D. Combined Effect of CVR and DG Penetration in the Voltage Profile of Low-Voltage Secondary Distribution Networks. *IEEE Trans. Power Deliv.* **2016**, *31*, 286–293. [CrossRef]
33. Singh, B.; Gyanish, B.J. Impact assessment of DG in distribution systems from minimization of total real power loss viewpoint by using optimal power flow algorithms. *Energy Rep.* **2018**, *4*, 407–417. [CrossRef]
34. Hraiz, M.D.; Garcia, J.A.M.; Jimenez Castaneda, R.; Muhsen, H. Optimal PV Size and Location to Reduce Active Power Losses While Achieving Very High Penetration Level with Improvement in Voltage Profile Using Modified Jaya Algorithm. *IEEE J. Photovolt.* **2020**, *10*, 1166–1174. [CrossRef]
35. Ravindran, S.; Victoire, T.A. A bio-geography-based algorithm for optimal siting and sizing of distributed generators with an effective power factor model. *Comput. Electr. Eng.* **2018**, *72*, 482–501. [CrossRef]
36. Essallah, S.; Khedher, A.; Bouallegue, A. Integration of distributed generation in electrical grid: Optimal placement and sizing under different load conditions. *Comput. Electr. Eng.* **2019**, *79*, 106461. [CrossRef]
37. Molver, I.; Chowdhury, S. Alternative approaches for analysing the impact of distributed generation on shunt compensated radial medium voltage networks. *Comput. Electr. Eng.* **2020**, *85*, 106676. [CrossRef]
38. Agajie, T.F.; Khan, B.; Guerrero, J.M.; Mahela, O.P. Reliability enhancement and voltage profile improvement of distribution network using optimal capacity allocation and placement of distributed energy resources. *Comput. Electr. Eng.* **2021**, *93*, 107295. [CrossRef]

39. Abujubbeh, M.; Fahrioglu, M.; Al-Turjman, F. Power loss reduction and voltage enhancement via distributed photovoltaic generation: Case study in North Cyprus. *Comput. Electr. Eng.* **2021**, *95*, 107432. [CrossRef]
40. Subramanyam, T.C.; Ram, S.T.; Subrahmanyam, J.B. Dual stage approach for optimal sizing and siting of fuel cell in distributed generation systems. *Comput. Electr. Eng.* **2018**, *69*, 676–689. [CrossRef]
41. Salimon, S.A.; Adepoju, G.A.; Adebayo, I.G.; Adewuyi, O.B. Comparative assessment of techno-economic and environmental benefits in optimal allocation of distributed generators in distribution networks. *Sci. Afr.* **2023**, *19*, e01546. [CrossRef]
42. Kakran, S.; Chanana, S. Smart operations of smart grids integrated with distributed generation: A review. *Renew. Sustain. Energy Rev.* **2018**, *81*, 524–535. [CrossRef]
43. Marini, A.; Mortazavi, S.S.; Piegari, L.; Ghazizadeh, M.S. An efficient graph-based power flow algorithm for electrical distribution systems with a comprehensive modeling of distributed generations. *Electr. Power Syst. Res.* **2019**, *170*, 229–243. [CrossRef]
44. Hu, S.; Xiang, Y.; Zhang, X.; Liu, J.; Wang, R.; Hong, B. Reactive power operability of distributed energy resources for voltage stability of distribution networks. *J. Mod. Power Syst. Clean Energy* **2019**, *7*, 851–861. [CrossRef]
45. Gupta, A.R.; Kumar, A. Impact of various load models on D-STATCOM allocation in DNO operated distribution network. *Procedia Comput. Sci.* **2018**, *125*, 862–870. [CrossRef]
46. Salimon, S.A.; Baruwa, A.A.; Amuda, S.O.; Adeleke, H.A. Optimal placement and sizing of capacitors in radial distribution systems: A two-stage method. *J. Eng. Res. Rep.* **2020**, *19*, 31–43. [CrossRef]
47. Bajaj, M.; Singh, A.K. Optimal design of passive power filter for enhancing the harmonic-constrained hosting capacity of renewable DG systems. *Comput. Electr. Eng.* **2022**, *97*, 107646. [CrossRef]
48. Meera, P.S.; Hemamalini, S. Optimal Siting of Distributed Generators in a Distribution Network using Artificial Immune System. *Int. J. Electr. Comput. Eng* **2017**, *7*, 641–649.
49. Reddy, P.D.P.; Reddy, V.C.V.; Manohar, T.G. Optimal renewable resources placement in distribution networks by combined power loss index and whale optimization algorithms. *J. Electr. Syst. Inf. Technol.* **2018**, *5*, 175–191.
50. Hassan, A.; Fahmy, F.; Nafeh, A.; Abuelmagd, M. Genetic single objective optimization for sizing and allocation of renewable DG systems. *Int. J. Sustain. Energy* **2015**, *36*, 545–562. [CrossRef]
51. Kansal, S.; Kumar, V.; Tyagi, B. Hybrid approach for optimal placement of multiple DGs of multiple types in distribution networks. *Int. J. Electr. Power Energy Syst.* **2016**, *75*, 226–235. [CrossRef]
52. Sudabattula, S.; Kowsalya, M. Distributed energy resources allocation using flower pollination algorithm in radial distribution systems. *Energy Procedia* **2016**, *103*, 76–81. [CrossRef]
53. Prakash, D.B.; Lakshminarayana, C. Multiple DG placements in radial distribution system for multi objectives using Whale Optimization Algorithm. *Alex. Eng. J.* **2018**, *57*, 2797–2806. [CrossRef]
54. El-Fergany, A. Optimal allocation of multi-type distributed generators using backtracking search optimization algorithm. *Int. J. Electr. Power Energy Syst.* **2015**, *64*, 1197–1205. [CrossRef]
55. Kashyap, M.; Kansal, S.; Verma, R. Sizing and allocation of DGs in a passive distribution network under various loading scenarios. *Electr. Power Syst. Res.* **2022**, *209*, 108046. [CrossRef]
56. Salimon, S.A.; Suuti, K.A.; Adeleke, H.A.; Ojo, K.E.; Aderinko, H.A. Impact of optimal placement and sizing of capacitors on radial distribution network using cuckoo search algorithm. *IOSR J. Electr. Electron. Eng.* **2020**, *15*, 39–49.
57. Okelola, M.O.; Adebiyi, O.W.; Salimon, S.A.; Ayanlade, S.O.; Amoo, A.L. Optimal sizing and placement of shunt capacitors on the distribution system using whale optimization algorithm. *Niger. J. Technol. Dev.* **2022**, *19*, 39–47. [CrossRef]
58. Abdelaziz, A.Y.; Hegazy, Y.G.; El-Khattam, W.; Othman, M.M. A Multi-objective Optimization for Sizing and Placement of Voltage-controlled Distributed Generation Using Supervised Big Bang–Big Crunch Method. *Electr. Power Compon. Syst.* **2015**, *43*, 105–117. [CrossRef]
59. Mahmoud, K.; Yorino, N.; Ahmed, A. Optimal distributed generation allocation in distribution systems for loss minimization. *IEEE Trans. Power Syst.* **2016**, *31*, 960–969. [CrossRef]
60. Mohamed, A.A.; Kamel, S.; Selim, A.; Khurshaid, T.; Rhee, S.B. Developing a Hybrid Approach Based on Analytical and Metaheuristic Optimization Algorithms for the Optimization of Renewable DG Allocation Considering Various Types of Loads. *Sustainability* **2021**, *13*, 4447. [CrossRef]
61. Elseify, M.A.; Kamel, S.; Abdel-Mawgoud, H.; Elattar, E.E. A Novel Approach Based on Honey Badger Algorithm for Optimal Allocation of Multiple DG and Capacitor in Radial Distribution Networks Considering Power Loss Sensitivity. *Mathematics* **2022**, *10*, 2081. [CrossRef]
62. Nowdeh, S.A.; Davoudkhani, I.F.; Moghaddam, M.H.; Najmi, E.S.; Abdelaziz, A.Y.; Ahmadi, A.; Razavi, S.E.; Gandoman, F.H. Fuzzy multi-objective placement of renewable energy sources in distribution system with objective of loss reduction and reliability improvement using a novel hybrid method. *Appl. Soft Comput.* **2019**, *77*, 761–779. [CrossRef]